Journal of Computational Physics **153,** 160–202 (1999)
Article ID jcph.1999.6272, available online at http://www.idealibrary.com on IDEAL®

Integral Equation Method for Coupled Schrödinger Equations

R. A. Gonzales,* S.-Y. Kang,* I. Koltracht,* and G. Rawitscher†

**Department of Mathematics and †Department of Physics, University of Connecticut, Storrs, Connecticut 06269*

Received June 10, 1998; revised April 2, 1999

A new integral equation method for the numerical solution of the radial Schrödinger equation in one dimension, developed by the authors (1997, *J. Comput. Phys.* **134**, 134), is extended to systems of coupled Schrödinger equations with both positive and negative channel energies. The method, carried out in configuration space, is based on the conversion of differential equations into a system of integral equations together with the application of a spectral type Clenshaw–Curtis quadrature. An accompanying general multichannel FORTRAN code is available upon request.

1. INTRODUCTION

This paper extends the technique for solving a single channel one-dimensional Schrödinger equation presented in Gonzales *et al.* [1] to coupled Schrödinger equations. The advantage of solving a system of integral equations rather than differential equations is the enhanced numerical stability. The usual disadvantage of integral equations is that the associated matrices are not sparse, making the numerical method computationally "expensive," in contrast to differential equation techniques, which lead to sparse matrices. In our method the non-sparse matrix difficulty is circumvented by subdividing the full interval into partitions. In each partition our matrices are non-sparse, but they are of small dimension (given by the number of support points, usually 16, in each partition, times the number of channels). The procedure of combining the local solutions in each partition into a global solution is accomplished by a big matrix which is sparse, however. Furthermore, since the approximation of the local solutions in each partition is super-algebraic in accuracy (we use interpolating polynomials at Chebyshev points), and since the local error in each partition is easily determined, our method allows for a small overall number of discretization points, which in turn minimizes the accumulation of round-off errors, already small for the integral equation method.

The kernel of the integral equation is obtained from Green's functions multiplied by the potential matrix. The former are written in terms of simple sine and cosine functions of

0021-9991/99 $30.00

the wave number in each channel times the radial distance. In the negative energy channels the corresponding functions are made out of hyperbolic sines and decaying exponentials. The numerical values of these latter functions can become very disparate and hence might lead to loss of accuracy. This problem is overcome by a special scaling procedure, as is explained in detail in the text.

Another potential difficulty consists in satisfying the asymptotic boundary conditions for the case that the angular momentum number $\ell \neq 0$. In order to avoid having to integrate out to distances so large that the centripetal potential, $\ell(\ell+1)/r^2$ is negligible, it is preferable to integrate out only to distances where the other potentials are negligible, and there match the solution to the appropriate Bessel or Coulomb functions. In order to achieve the boundary conditions of outgoing waves in all channels other than the incident channel, it is necessary to solve the coupled integral equations as many times as there are positive energy channels. We demonstrate in this paper that the matrix which performs the appropriate linear combination of theses solutions is well conditioned, hence the appropriate boundary conditions can be achieved without undue loss of accuracy.

In summary, the extension of the integral equation method from one to several coupled channels requires an examination of how to achieve the appropriate boundary conditions, both in the positive and the negative channels, and this, together with several numerical demonstrations, is the main content of the present paper.

Our method is expected to be well suited for situations where the potentials decay slowly with distance, where many channels of both positive and negative energies occur, and where high accuracy is required. An example is the description of the collision of atoms at low incident energies, corresponding to temperatures of micro-Kelvin. This situation occurs in the Bose–Einstein condensation of atoms, and in the photo-association of atoms into molecules previous to the condensation of the molecules [2]. Other applications are likely to occur for atomic or nuclear many-body systems, either confined to a lattice or in free space in the case that the treatment of such systems can be done by the mean field approximation (also called Hartree–Fock), which leads to systems of a non-linear Schroedinger equation [3]. The solution usually can be achieved iteratively, by means of inhomogeneous terms introduced into the two-body equations. As shown in the Appendix, our system of integral equations can be easily extended to include inhomogeneous terms, in such a way that most parts of the numerical calculations need not be repeated after each iteration. Hence our method should be suitable for carrying out the Hartree–Fock approximation.

The system of equations that we wish to solve is of the form

$$\left[-\frac{d^2}{dr^2} I + \frac{1}{r^2} L + \bar{V}(r)\right] R(r) = \bar{E} R(r), \qquad 0 < r < \infty, R(0) = 0, \tag{1}$$

where I is the $p \times p$ identity matrix, p is the number of channels coupled to each other, $L = \mathrm{diag}(l_1(l_1+1), \ldots, l_p(l_p+1))$, is the diagonal matrix of angular momentum numbers, $\bar{V}(r) = (v_{i,j}(r))_{i,j=1}^{p}$ is the potential matrix, $\bar{E} = \mathrm{diag}(k_1^2, \ldots, k_s^2, -k_{s+1}^2, \ldots, -k_p^2)$, $k_j > 0$, $j = 1, \ldots, p$, is the diagonal energy matrix obtained from the wave numbers k_j in each channel, and $R(r) = (R_1(r), \ldots, R_p(r))^T$ is the p-vector valued wave function to be found at each radial distance r.

We assume here that the number of positive energy channels, s, is ≥ 1, and that $\bar{V}(r)$ is continuous on $(0, \infty)$ and has the following behavior at the endpoints: it tends to zero as

fast or faster than $1/r^2$, as $r \to \infty$, and as $r \to 0$ it does not grow faster than $1/r$. Under these conditions on $\bar{V}(r)$, the initial value problem (1) has a unique bounded solution on $(0, \infty)$ (see Faddeev [4] and references therein), satisfying the asymptotic conditions

$$\lim_{r\to\infty}\left(R_1(r) - \sin\left(k_1 r - \frac{\ell_1\pi}{2}\right) - \omega_1 \exp\left(i\left(k_1 r - \frac{\ell_1\pi}{2}\right)\right)\right) = 0, \tag{2}$$

$$\lim_{r\to\infty}\left(R_j(r) - \omega_j \exp\left(i\left(k_j r - \frac{\ell_j\pi}{2}\right)\right)\right) = 0, \qquad j = 2, \ldots, s, \tag{3}$$

$$\lim_{r\to\infty}\left(R_j(r) - \omega_j \exp(-k_j r)\right) = 0, \qquad j = s+1, \ldots, p, \tag{4}$$

where ω_j are unknown constants uniquely determined by the problem together with the solution $R(r)$. A more detailed description of the Schrödinger equation and its reduction to systems of ODEs can be found, e.g., in Landau [5] and Schiff [6].

In our treatment we replace the boundary value problem (1)–(4) with a system of coupled integral equations, solved in the radial interval $[0, T]$ for s different right hand sides,

$$\Psi_j(r) + K^{-1}S(r)\int_r^T C(r')V(r')\Psi_j(r')\,dr' + k^{-1}C(r)\int_0^r S(r')V(r')\Psi_j(r')\,dr' = U_j(r), \qquad 0 < r < T,\ j = 1, \ldots, s, \tag{5}$$

where

$$V(r) = \bar{V}(r) + \frac{1}{r^2}L,$$

$$K^{-1} = \operatorname{diag}\left(k_1^{-1}, \ldots, k_s^{-1}, k_{s+1}^{-1}, \ldots, k_p^{-1}\right),$$

$$S(r) = \operatorname{diag}(\sin(k_1 r), \ldots, \sin(k_s r), \sinh(k_{s+1} r), \ldots, \sinh(k_p r)),$$

$$C(r) = \operatorname{diag}(\cos(k_1 r), \ldots, \cos(k_s r), \exp(-k_{s+1} r), \ldots, \exp(-k_p r))),$$

and

$$U_j(r) = (\delta_{1j}\sin(k_1 r), \ldots, \delta_{sj}\sin(k_s r), 0, \ldots, 0)^T.$$

Here sinh denotes the hyperbolic sine, $\sinh(t) = (\exp(t) - \exp(-t))/2$, and δ is the usual Kronecker symbol. The solution of (1)–(4) is obtained as a linear combination of $\Psi_1(r), \ldots, \Psi_s(r)$ as explained in the following section.

The integral equation is discretized via a spectral type composite Clenshaw–Curtis numerical quadrature. This method leads to a narrow banded linear system of equations. The complexity of solving this system is linear in the number of support points. The latter is achieved by using the special semiseparable structure of the kernel of the integral equation in configuration space. In our examples we observe numerical behavior typical for spectral methods, where after reaching a sufficient number of discretization points the error drops rapidly to the machine precision. Due to the well-conditioning of integral equations further increase in the number of discretization points does produce only very slow accumulation of rounding errors.

The paper is organized as follows. In Section 2 we derive the equivalent integral equation formulation. In Section 3 we show that the global solution can be found as a linear combination of local solutions of integral equations restricted to small subintervals of the partition of the whole radial interval. Each local equation is discretized using the Clenshaw–Curtis quadrature with a very limited number of support points (16 in our implementation), as described in Section 4. In Section 5 we describe results of our numerical experiments and compare them with the results obtained via the Numerov, finite difference type method.

It is appropriate to clarify here that the main purpose of these experiments is to examine numerical difficulties arising from the transition from one channel to coupled channels. Therefore the simple Numerov method is chosen for numerical comparisons. An accuracy comparison with a more advanced variable step size finite difference method of Raptis and Cash was done in [1]. The additional difficulty in the multichannel case arises from combining particular solutions of the system of Schrödinger equations to satisfy required asymptotic conditions and to suppress exponentially growing solutions. It is known and is further illustrated in Section 5, Fig. 1, that an unlucky choice of initial guesses in finite difference methods may lead to particular solutions which become increasingly linearly dependent, thus causing additional loss of accuracy. Our proposed "integral equation method" (IEM) results in well conditioned matching matrices as is illustrated with numerical examples.

In the Appendix we present two new results concerning the single channel case obtained since [1] was published, both relevant to the coupled channel case. In the first one we replace the general semiseparable kernel with a Volterra semiseparable kernel which leads to a more effective algorithm, both time and memory wise. The FORTRAN code for solving a coupled channel system of Schrödinger equations with at least one positive channel and an arbitrary number of positive and negative channels is based on this Volterra approach. The code is available now upon request and will be submitted to the journal *Computer Physics Communications*. The second result is the extension of IEM to the inhomogeneous case which occurs when part of the interaction is taken into account iteratively. Summary and conclusions are presented before the Appendixes.

2. INTEGRAL EQUATION FORMULATION

We wish to solve the system of radial Schrödinger equations

$$\left[-\frac{\hbar^2}{2m}\frac{d^2}{dr^2}I + \frac{\hbar^2}{2mr^2}L + \mathcal{V}(r)\right]R(r) = E\,R(r) \tag{6}$$

subject to the conditions (2)–(4). Here r is the radial distance of the particle of mass m to the scattering center, E is the diagonal matrix of positive and negative energies, and L is the diagonal matrix of angular momentum numbers as defined in the Introduction. $\mathcal{V}$ is the matrix of diagonal and coupling potentials and $\hbar$ is Planck's constant divided by 2π. With $\bar{E} = (2m/\hbar^2)E$, we can write (6) as

$$\left[\frac{d^2}{dr^2}I + \bar{E}\right]R_\ell(r) = V(r)R_\ell(r), \tag{7}$$

where $V(r) = L/r^2 + \bar{V}(r)$ and $\bar{V}(r) = (2m/\hbar^2)\mathcal{V}(r)$.

The following proposition shows that the solution of this system of differential equations also satisfies the system of integral equations (5). It is assumed that T is chosen sufficiently

large such that the potential $\bar{V}(r)$ and the decaying solutions in negative energy channels times their respective coupling potentials are numerically negligible for $r \geq T$. In the proposition, the symbol i in the exponentials in Eqs. (9) and (10) denotes $\sqrt{-1}$, not to be confused with the index $i = 1, \ldots, s$ subsequentially used throughout the paper.

PROPOSITION 1. *Let $R^{(i)}(r)$, $i = 1, \ldots, s$, be the unique solutions of the coupled system of Schrödinger equations,*

$$\left[\frac{d^2}{dr^2} I + K\right] R^{(i)}(r) = V(r) R^{(i)}(r), \qquad 0 < r < \infty, R^{(i)}(0) = 0, \tag{8}$$

satisfying the asymptotic conditions,

$$\lim_{r\to\infty} \left(R_i^{(i)}(r) - \sin\left(k_i r - \frac{\ell_i \pi}{2}\right) - \omega_i^{(i)} \exp\left(i\left(k_i r - \frac{\ell_i \pi}{2}\right)\right)\right) = 0, \tag{9}$$

$$\lim_{r\to\infty} \left(R_j^{(i)}(r) - \omega_j^{(i)} \exp\left(i\left(k_j r - \frac{\ell_j \pi}{2}\right)\right)\right) = 0, \qquad j = 1, \ldots, s, j \neq i, \tag{10}$$

$$\lim_{r\to\infty} \left(R_j^{(i)}(r) - \omega_j^{(i)} \exp(-k_j r)\right) = 0, \qquad j = s+1, \ldots, p, \tag{11}$$

where $R_j^{(i)}(r)$ denotes the jth component of the solution $R^{(i)}$. Let

$$\Phi^{(i)}(r) = \begin{bmatrix} \sin(k_1 r) R_1^{(i)}(r) + \frac{1}{k_1} \cos(k_1 r) R_1^{(i)'}(r) \\ \vdots \\ \sin(k_s r) R_s^{(i)}(r) + \frac{1}{k_s} \cos(k_s r) R_s^{(i)'}(r) \\ \exp(-k_{s+1} r)\left(R_{s+1}^{(i)}(r) + \frac{1}{k_{s+1}} R_{s+1}^{(i)'}(r)\right) \\ \vdots \\ \exp(-k_p r)\left(R_p^{(i)}(r) + \frac{1}{k_p} R_p^{(i)'}(r)\right) \end{bmatrix}, \qquad 0 < r < \infty. \tag{12}$$

Then the system of integral equations

$$\Psi_i(r) + K^{-1} S(r) \int_r^T C(r') V(r') \Psi_i(r')\, dr' + K^{-1} C(r) \int_0^r S(r') V(r') \Psi_i(r')\, dr'$$
$$= S(r) \Phi^{(i)}(T), \qquad 0 < r < T, \tag{13}$$

has a solution $\Psi_i = R^{(i)}$. Conversely, a solution of the system of integral equations

$$\Psi(r) + K^{-1} S(r) \int_r^T C(r') V(r') \Psi(r')\, dr' + K^{-1} C(r) \int_0^r S(r') V(r') \Psi(r')\, dr'$$
$$= S(r) \begin{bmatrix} \alpha_1 \\ \vdots \\ \alpha_p \end{bmatrix}, \qquad 0 < r < T, \tag{14}$$

satisfies (8) *for any choice of constants $\alpha_1, \ldots, \alpha_p$.*

Proof. Since for r close to T the system (8) decouples into p independent Bessel equations it follows that $R^{(1)}, \dots, R^{(s)}$ are linearly independent p-vector valued functions on $[0, T]$.

Let $R^{(i)}$ satisfy (8)–(11) and consider

$$\mu^{(i)}(r) = R^{(i)}(r) + K^{-1}S(r)\int_r^T C(r')V(r')R^{(i)}(r')\,dr' + K^{-1}C(r)\int_0^r S(r')V(r')R^{(i)}(r')\,dr', \qquad 0 < r < T.$$

Differentiating we get

$$\mu^{(i)'}(r) = R^{(i)'}(r) + \bar{C}(r)\int_r^T C(r')V(r')R^{(i)}(r')\,dr' - \bar{S}(r)\int_0^r S(r')V(r')R^{(i)}(r')\,dr', \qquad 0 < r < T,$$

where $\bar{S}(r) = \operatorname{diag}(\sin(k_1 r), \dots, \sin(k_s r), \exp(-k_{s+1}r), \dots, \exp(-k_p r))$ and $\bar{C}(r) = \operatorname{diag}(\cos(k_1 r), \dots, \cos(k_s r), \cosh(k_{s+1}r), \dots, \cosh(k_p r))$. Differentiating one more time and using (7) we obtain

$$\mu^{(i)''}(r) = -\bar{E}\mu^{(i)}(r).$$

Thus, $\mu^{(i)}(r) = S(r)(\alpha_1, \dots, \alpha_p)^T + C(r)(\beta_1, \dots, \beta_p)^T$. Since $\mu^{(i)}(0) = 0$ it follows that $\mu^{(i)}(r) = S(r)(\alpha_1, \dots, \alpha_p)^T$. To find $\alpha_1, \dots, \alpha_p$, multiply $\mu^{(i)}(T)$ by

$$K\operatorname{diag}(\sin(k_1 T), \dots, \sin(k_s T), 1, \dots, 1),$$

multiply $\mu^{(i)'}(T)$ by

$$\operatorname{diag}(\cos(k_1 T), \dots, \cos(k_s T), 1, \dots, 1)$$

and add to get

$$\begin{bmatrix} \alpha_1 \\ \vdots \\ \alpha_p \end{bmatrix} = \Phi^{(i)}(T).$$

Conversely, if $\Psi(r)$ is a solution of (14) then it is clear that $\Psi(0) = 0$ and differentiating (13) twice it is easy to see that $\Psi(r)$ satisfies the differential equation as well. The proposition is proved. ∎

Note that since for sufficiently large T the components of the solution $R^{(i)}$ corresponding to the negative energy channels, $j = s+1, \dots, p$ are negligibly small, it follows from substituting $R^{(i)}$ for Ψ_i into (13) that the corresponding components in the left hand side of (13) and hence the corresponding components in the right hand side of (13), namely,

$$\exp(-k_j T)\left(R_p^{(i)}(T) + \frac{1}{k_j}R_j^{(i)'}(T)\right)\sinh(k_j r), \qquad j = s+1, \dots, p,$$

are also negligibly small. Therefore in our practical implementation we set them to zero. We also assume that the vectors

$$\Phi_0^{(i)}(T) = \begin{bmatrix} \sin(k_1 T) R_1^{(i)}(T) + \frac{1}{k_1} \cos(k_1 T) R_1^{(i)'}(T) \\ \vdots \\ \sin(k_s T) R_s^{(i)}(T) + \frac{1}{k_s} \cos(k_s T) R_s^{(i)'}(T) \end{bmatrix}, \qquad i = 1, \ldots, s,$$

are linearly independent. Therefore we chose the natural coordinate basis for the span of $\Phi_0^{(1)}(T), \ldots, \Phi_0^{(s)}(T)$ and instead of solving Eq. (14) with α_i given by Φ_i, we solve numerically for $j = 1, \ldots, s$ the following systems of integral equations,

$$\Psi_j(r) + K^{-1} S(r) \int_r^T C(r') V(r') \Psi_j(r')\, dr' + K^{-1} C(r) \int_r^T S(r') V(r') \Psi_j(r')\, dr' = U_j(r), \qquad 0 < r < T,\ j = 1, \ldots, s, \tag{15}$$

where U_j is as defined in (5). The quantities Ψ_j, $j = 1, \ldots, s$, are column vectors of length p. However, none of them obey the desired boundary condition (2)–(4), unless $L = 0$ and $j = 1$. In the general case the boundary conditions (2)–(4) are achieved through an appropriate linear combination of $\Psi_1, \ldots, \Psi_s$ as explained below. We do not anticipate numerical difficulties in the case when T is near T_0 for which $\Phi_0^{(1)}(T_0), \ldots, \Phi_0^{(s)}(T_0)$ are linearly dependent. In this case, the computed $\Psi_j(r)$ become large, but retain high relative accuracy. This is because the solutions of the homogeneous equation (14) with zeros in the right hand side also satisfy (8). It is similar to the case of the inverse iteration algorithm for computing eigenvectors, where one solves a nearly singular linear system of equations, for which the solution is an approximate eigenvector, see Golub and Van Loan [11, Sect. 7.6].

Next we show how to find $R(r) = R^{(1)}(r)$ in terms of $\Psi_1, \ldots, \Psi_s$. For $r \approx T$ the system (1)–(4) decouples into independent Riccati–Bessel equations for the components of the vector R,

$$\left[\frac{d^2}{dr^2} - \frac{\ell_i(\ell_i + 1)}{r^2} + k_i^2 \right] R_i(r) = 0, \qquad i = 1, \ldots, s,$$

and similar equations for $i = s + 1, \ldots, p$. Each of the first s equations has a pair of linearly independent solutions, the Riccati–Bessel functions,

$$F_{l_i}(r) = z j_{l_i}(z) = \sqrt{\frac{\pi z}{2}}\, J_{l_i + \frac{1}{2}}(z)$$

and

$$G_{l_i}(r) = -z y_{l_i}(z) = -\sqrt{\frac{\pi z}{2}}\, Y_{l_i + \frac{1}{2}}(z),$$

where $z = k_i r$ (cf. Abramovitz and Stegun [12]). Since near T the functions $\Psi_1, \ldots, \Psi_s$

satisfy this decoupled system of Riccati–Bessel equations, it follows that

$$\begin{bmatrix} \Psi_{1j}(r) \\ \vdots \\ \Psi_{sj}(r) \end{bmatrix} = \begin{bmatrix} \alpha_{ij} F_{l_1}(r) + \beta_{1j} G_{l_1}(r) \\ \vdots \\ \alpha_{sj} F_{l_s}(r) + \beta_{sj} G_{l_s}(r) \end{bmatrix}.$$

To find α_{ij} and β_{ij} differentiate

$$\Psi_{ij}(r) = \alpha_{ij} F_{l_i}(r) + \beta_{ij} G_{l_i}(r)$$

in r to get

$$\Psi'_{ij}(r) = \alpha_{ij} F'_{l_i}(r) + \beta_{ij} G'_{l_i}(r).$$

Multiply the first equation by $G'_{l_i}(r)$ and the second by $G_{l_i}(r)$, subtract and substitute $r = T$ to get

$$\alpha_{ij} = \frac{\Psi_{ij}(T) G'_{l_i}(T) - \Psi'_{ij}(T) G_{l_i}(T)}{F_{l_i}(T) G'_{l_i}(T) - F'_{l_i}(T) G_{l_i}(T)} \tag{16}$$

and in a similar way,

$$\beta_{ij} = -\frac{\Psi_{ij}(T) F'_{l_i}(T) - \Psi'_{ij}(T) F_{l_i}(T)}{F_{l_i}(T) G'_{l_i}(T) - F'_{l_i}(T) G_{l_i}(T)}. \tag{17}$$

Asymptotically, the Riccati–Bessel functions $F_\ell(r)$ and $G_\ell(r)$ behave like $\sin(kr - \frac{\ell\pi}{2})$ and $\cos(kr - \frac{\ell\pi}{2})$, respectively. Under our assumptions $R(r)$ is a unique linear combination of $\Psi_1, \ldots, \Psi_s$,

$$R = x_1 \Psi_1 + \cdots + x_s \Psi_s.$$

Therefore it follows from (2) and (3) that asymptotically this linear combination behaves as

$$\sum_{j=1}^{s} x_j \begin{bmatrix} \alpha_{1j} F_{l_1}(r) + \beta_{1j} G_{l_1}(r) \\ \vdots \\ \alpha_{sj} F_{l_s}(r) + \beta_{sj} G_{l_s}(r) \end{bmatrix} = \sum_{j=1}^{s} x_j \begin{bmatrix} \alpha_{1j} \sin\bigl(k_1 r - \frac{\ell_1\pi}{2}\bigr) + \beta_{1j} \cos\bigl(k_1 r - \frac{\ell_1\pi}{2}\bigr) \\ \vdots \\ \alpha_{sj} \sin\bigl(k_s r - \frac{\ell_s\pi}{2}\bigr) + \beta_{sj} \cos\bigl(k_s r - \frac{\ell_s\pi}{2}\bigr) \end{bmatrix}$$

while our desired solution behaves as

$$\begin{bmatrix} \sin\bigl(k_1 r - \frac{\ell_1\pi}{2}\bigr) + \omega_1\bigl(\cos\bigl(k_1 r - \frac{\ell_1\pi}{2}\bigr) + i \sin\bigl(k_1 r - \frac{\ell_1\pi}{2}\bigr)\bigr) \\ \vdots \\ \omega_s\bigl(\cos\bigl(k_s r - \frac{\ell_s\pi}{2}\bigr) + i \sin\bigl(k_s r - \frac{\ell_s\pi}{2}\bigr)\bigr) \end{bmatrix}$$

$$= \begin{bmatrix} (1 + i\omega_1) \sin\bigl(k_1 r - \frac{\ell_1\pi}{2}\bigr) + \omega_1 \cos\bigl(k_1 r - \frac{\ell_1\pi}{2}\bigr) \\ \vdots \\ i\omega_s \sin\bigl(k_s r - \frac{\ell_s\pi}{2}\bigr) + \omega_s \cos\bigl(k_s r - \frac{\ell_s\pi}{2}\bigr) \end{bmatrix}.$$

Comparing the entries in the first position we get

$$\sum_{j=1}^{s} \alpha_{1j} x_j = 1 + i\omega_1, \qquad \sum_{j=1}^{s} \beta_{1j} x_j = \omega_1.$$

Excluding ω_1, we obtain

$$\sum_{j=1}^{s} \alpha_{1j} x_j - i \sum_{j=1}^{s} \beta_{1j} x_j = 1.$$

In a similar way, excluding $\omega_2, \ldots, \omega_s$ from equations corresponding to positions 2 to s we obtain the following linear system of equations for $x_1, \ldots, x_s$,

$$\begin{bmatrix} \alpha_{11} - i\beta_{11} & \cdots & \alpha_{1s} - i\beta_{1s} \\ \vdots & \vdots & \vdots \\ \alpha_{s1} - i\beta_{s1} & \cdots & \alpha_{ss} - i\beta_{ss} \end{bmatrix} \begin{bmatrix} x_1 \\ \vdots \\ x_s \end{bmatrix} = \begin{bmatrix} 1 \\ \vdots \\ 0 \end{bmatrix}. \tag{18}$$

The asymptotic constants $\omega_1, \ldots, \omega_s$ are now given by

$$\begin{bmatrix} \omega_1 \\ \vdots \\ \omega_s \end{bmatrix} = \begin{bmatrix} \beta_{11} & \cdots & \beta_{1s} \\ \vdots & \vdots & \vdots \\ \beta_{s1} & \cdots & \beta_{ss} \end{bmatrix} \begin{bmatrix} x_1 \\ \vdots \\ x_s \end{bmatrix}. \tag{19}$$

The asymptotic constants $\omega_{s+1}, \ldots, \omega_p$ can be found in a similar way; they usually are, however, of little interest to physicists.

We remark that instead of matching to (2) and (3), one can match to the following asymptotic condition, $\delta_{1j} \sin(k_i r - l_i \pi/2) + \rho_i \cos(k_i r - l_i \pi/2)$, $i = 1, \ldots, s$. Here the ρ_i's are elements of the so-called scattering K-matrix, while the ω's are elements of the Ω-matrix, with $\Omega = -2K(1 - iK)^{-1}$, which is related to the scattering S-matrix via $S = I - i\Omega$. In this case there is no need for complex arithmetic. The only change is that instead of (18) we solve

$$\begin{bmatrix} \alpha_{11} & \cdots & \alpha_{1s} \\ \vdots & \vdots & \vdots \\ \alpha_{s1} & \cdots & \alpha_{ss} \end{bmatrix} \begin{bmatrix} x_1 \\ \vdots \\ x_s \end{bmatrix} = \begin{bmatrix} 1 \\ \vdots \\ 0 \end{bmatrix} \tag{20}$$

and obtain $p_1, \ldots, p_s$ from (19) instead of $\omega_1, \ldots, \omega_s$. We remark that the coefficient matrix in (20) can become singular, as opposed to (18). This means that the phase shifts $\phi_i = \arctan(\rho_i)$ go through multiples of $\pi/2$, which is of some interest to physicists. For our numerical applications we implemented (20) rather than (18) and, in fact, detected a particular case of large ρ_i as reported in Section 5 below. Large ρ_i had no visible ill effect on the overall accuracy of computation.

The summary of our general algorithm is as follows.

1. Solve (15) for $j = 1, \ldots, s$.
2. Compute α_{ij} and β_{ij}, $i, j = 1, \ldots, s$, from (16) and (17).
3. Solve (20) and compute $\rho_1, \ldots, \rho_s$ from (19).

In our numerical implementation described below, the functions $\Psi_j(r)$ are found as piecewise polynomials at Chebyshev support points. The values of their derivatives at $r = T$ are obtained by differentiating the integral equations (15) and substituting $r = T$. The values of Riccati–Bessel functions and their derivatives are readily available from recursive relations satisfied by these functions, or from a scientific subroutine library.

3. LOCAL SOLUTIONS

To avoid notational complexity we do not use special symbols to distinguish vectors from matrices. Instead we alert the reader that the quantities Ψ, A, B, e are vectors, and K^{-1}, V, C, S, Y, Z, M, I, E (and their products) are matrices.

Because of the semiseparable structure of the kernel of the integral equation (15), the Clenshaw–Curtis quadrature, which gives at no extra cost the whole anti-derivative function, is for our purposes the most appropriate method for discretizing (15). This quadrature is based on the interpolation of the integrand with a polynomial at Chebyshev support points. Since the length of the interval of integration, T, may require many support points, and in order to avoid working with high degree polynomials, we use the composite Clenshaw–Curtis quadrature suggested by Greengard and Rokhlin [9], by partitioning $[0, T]$ into sufficiently small subintervals. The second and equally important reason for partitioning the interval $[0, T]$ into smaller size subintervals and restricting the integral equation to each of them is that in the negative energy channels, $k = s + 1, \ldots, p$, the kernel contains an exponentially growing component $\sinh(kr)$. This component can be scaled down on subintervals of partition as will be explained after Eq. (34) below. A third important reason is that the procedure of obtaining the global solution Ψ out of the local solutions in each partition leads to a narrow banded matrix, whose inversion only requires an effort proportional to the number of partitions. The procedure will now be described.

Each partition will be denoted by the subscript i, $i = 1, \ldots, m$. For the sake of notational simplicity, we omit from now on the index j in Y_i and Z_i and in other quantities, such as A_i and B_i below, whenever it does not cause any ambiguity.

Consider the family of restricted integrad equations in each partition, i, for two matrix valued functions, $Y(r)$ and $Z(r)$,

$$Y_i(r) + K^{-1}S(r)\int_r^{b_i} C(r')V(r')Y_i(r')\,dr' + K^{-1}C(r)\int_{b_{i-1}}^{r} S(r')V(r')Y_i(r')\,dr' = S(r), \qquad b_{i-1} \le r \le b_i, \tag{21}$$

and

$$Z_i(r) + K^{-1}S(r)\int_r^{b_i} C(r')V(r')Z_i(r')\,dr' + K^{-1}C(r)\int_{b_{i-1}}^{r} S(r')V(r')Z_i(r')\,dr' = C(r), \qquad b_{i-1} \le r \le b_i, \tag{22}$$

respectively. Here $b_0 = 0 < b_1 < \cdots < b_{m-1} < b_m = T$ is some partitioning of the interval $[0, T]$. Each column of the matrices Y and Z corresponds to a local solution of the coupled Eq. (15), defined entirely in partition i, and "driven" by the corresponding column in the

matrix S or C, respectively. For a sufficiently fine partitioning, these equations have unique solutions Y_i and Z_i, which are $p \times p$ matrix valued functions. We now observe that the global solution $\Psi_j(r)$ of (15) on $[b_{i-1}, b_i]$ is a linear combination of Y_i and Z_i. Indeed, it follows from (15) that for $b_{i-1} \le r \le b_i$,

$$\begin{aligned}
&\Psi_j(r) + K^{-1}S(r)\int_r^{b_i} C(r')V(r')\Psi_j(r')\,dr' + K^{-1}C(r)\int_{b_{i-1}}^{r} S(r')V(r')\Psi_j(r')\,dr' \\
&\quad = S(r)\left(e_j - K^{-1}\int_{b_i}^{T} C(r')V(r')\Psi_j(r')\,dr'\right) \\
&\qquad + C(r)\left(-K^{-1}\int_0^{b_{i-1}} S(r')V(r')\Psi_j(r')\,dr'\right), \qquad (23)
\end{aligned}$$

where e_j denotes the unit coordinate vector with 1 in the jth position. For $i = 1, \ldots, m$, let the quantities in parentheses be denoted by

$$A_i = e_j - K^{-1}\int_{b_i}^{T} C(r')V(r')\Psi_j(r')\,dr' \qquad (24)$$

and

$$B_i = -K^{-1}\int_0^{b_{i-1}} S(r')V(r')\Psi_j(r')\,dr'. \qquad (25)$$

It follows from (21) and (22) that $Y_iA_i + Z_iB_i$ satisfies (23) and hence

$$\Psi_j(r) = Y_iA_i + Z_iB_i, \qquad b_{i-1} \le r \le b_i.$$

Assuming that Y_i and Z_i are known, we show now how to find A_i and B_i. Let us rewrite (24) as

$$A_i = e_j - K^{-1}\sum_{q=i+1}^{m}\int_{b_{q-1}}^{b_q} C(r')V(r')\Psi_j(r')\,dr'.$$

Since on $[b_{q-1}, b_q]$, $\Psi_j = Y_qA_q + Z_qB_q$, we can also write

$$A_i = e_j - \sum_{q=i+1}^{m}(CY_q)A_q - \sum_{q=i+1}^{m}(CZ_q)B_q, \qquad (26)$$

where, by definition,

$$(CY_q) = K^{-1}\int_{b_{q-1}}^{b_q} C(r')V(r')Y_q(r')\,dr', \qquad (27)$$

and

$$(CZ_q) = K^{-1} \int_{b_{q-1}}^{b_q} C(r')V(r')Z_q(r')\,dr'. \tag{28}$$

Similarly,

$$B_i = -\sum_{q=1}^{i-1}(SY_q)A_q - \sum_{q=1}^{i-1}(SZ_q)B_q, \tag{29}$$

with the $p \times p$ matrices (SY_q) and (SZ_q) given in each partition by

$$(SY_q) = K^{-1} \int_{b_{q-1}}^{b_q} S(r')V(r')Y_q(r')\,dr' \tag{30}$$

and

$$(SZ_q) = K^{-1} \int_{b_{q-1}}^{b_q} S(r')V(r')Z_q(r')\,dr'. \tag{31}$$

Note that $A_m = e_j$ and $B_1 = 0$. Combining (26) and (29) for $i = 1, \ldots, m$, we obtain the following system of linear equations for the A_i's and B_i's,

$$\begin{pmatrix} \Lambda_{11} & \Lambda_{12} \\ \Lambda_{21} & \Lambda_{22} \end{pmatrix} \begin{pmatrix} A_1 \\ A_2 \\ \vdots \\ A_m \\ B_1 \\ B_2 \\ \vdots \\ B_m \end{pmatrix} = \begin{pmatrix} e_j \\ e_j \\ \vdots \\ e_j \\ 0 \\ 0 \\ \vdots \\ 0 \end{pmatrix}, \tag{32}$$

where

$$\Lambda_{11} = \begin{pmatrix} I & CY_2 & CY_3 & \cdots & CY_m \\ & I & CY_3 & \cdots & CY_m \\ & & I & \ddots & CY_m \\ & & & \ddots & CY_m \\ 0 & & & & I \end{pmatrix},$$

$$\Lambda_{12} = \begin{pmatrix} 0 & CZ_2 & CZ_3 & \cdots & CZ_m \\ & 0 & CZ_3 & \cdots & CZ_m \\ & & 0 & \ddots & CZ_m \\ & & & \ddots & CZ_m \\ 0 & & & & 0 \end{pmatrix},$$

$$\Lambda_{21} = \begin{pmatrix} 0 & & & & 0 \\ SY_1 & \ddots & & & \\ SY_1 & \ddots & 0 & & \\ SY_1 & \cdots & SY_{m-2} & 0 & \\ SY_1 & \cdots & SY_{m-2} & SY_{m-1} & 0 \end{pmatrix},$$

and

$$\Lambda_{22} = \begin{pmatrix} I & & & & 0 \\ SZ_1 & \ddots & & & \\ SZ_1 & \ddots & I & & \\ SZ_1 & \cdots & SZ_{m-2} & I & \\ SZ_1 & \cdots & SZ_{m-2} & SZ_{m-1} & I \end{pmatrix}.$$

For notational convenience we henceforth omit the parentheses in definitions (27), (28), (30), and (31). The system of linear equations (32) has a unique solution because otherwise (15) would not be uniquely solvable. Using elementary row operations (e.g., subtracting the second row from the first, then the third row from the second, etc.) Eq. (32) can be transformed into a sparse system,

$$\begin{pmatrix} \Sigma_{11} & \Sigma_{12} \\ \Sigma_{21} & \Sigma_{22} \end{pmatrix} \begin{pmatrix} A_1 \\ A_2 \\ \vdots \\ A_m \\ B_1 \\ B_2 \\ \vdots \\ B_m \end{pmatrix} = \begin{pmatrix} 0 \\ 0 \\ \vdots \\ 0 \\ e_j \\ 0 \\ 0 \\ \vdots \\ 0 \end{pmatrix},$$

where

$$\Sigma_{11} = \begin{pmatrix} I & CY_2 - I & & & 0 \\ & I & CY_3 - I & & \\ & & I & \ddots & \\ & & & \ddots & CY_m - I \\ 0 & & & & I \end{pmatrix},$$

$$\Sigma_{12} = \begin{pmatrix} 0 & CZ_2 & & & 0 \\ & 0 & CZ_3 & & \\ & & 0 & \ddots & \\ & & & \ddots & CZ_m \\ 0 & & & & 0 \end{pmatrix},$$

$$\Sigma_{21} = \begin{pmatrix} 0 & & & & 0 \\ SY_1 & \ddots & & & \\ & \ddots & 0 & & \\ & & SY_{m-2} & 0 & \\ 0 & & & SY_{m-1} & 0. \end{pmatrix},$$

and

$$\Sigma_{22} = \begin{pmatrix} I & & & & 0 \\ SZ_1 - I & \ddots & & & \\ & \ddots & I & & \\ & & SZ_{m-2} - I & I & \\ 0 & & & SZ_{m-1} - I & I \end{pmatrix}.$$

In a compact form we rewrite this equation as

$$\mathcal{L}A = F. \tag{33}$$

Changing the order of the varibles, we can finally transform the coefficient matrix into the block tridiagonal system,

$$\begin{pmatrix} \mathbf{I} & \mathbf{M}_{12} & & & 0 \\ \mathbf{M}_{21} & \mathbf{I} & \mathbf{M}_{23} & & \\ & \mathbf{M}_{32} & \ddots & \ddots & \\ & & \ddots & \mathbf{I} & \mathbf{M}_{m-1,m} \\ 0 & & & \mathbf{M}_{m,m-1} & \mathbf{I} \end{pmatrix} \begin{pmatrix} A_1 \\ B_1 \\ A_2 \\ B_2 \\ \vdots \\ A_m \\ B_m \end{pmatrix} = \begin{pmatrix} 0 \\ 0 \\ \vdots \\ 0 \\ e_j \\ 0 \end{pmatrix}, \tag{34}$$

where each block is a $2p \times 2p$ matrix and with

$$\mathbf{M}_{i-1,i} = \begin{pmatrix} CY_i - I & CZ_i \\ 0 & 0 \end{pmatrix}, \qquad i = 2, \ldots, m,$$

and

$$\mathbf{M}_{i,i-1} = \begin{pmatrix} 0 & 0 \\ SY_{i-1} & SZ_{i-1} - I \end{pmatrix}, \qquad i = 2, \ldots, m.$$

The coefficient matrix in (34) is narrow banded and therefore, the Gaussian elimination with partial pivoting (see [11, Sect. 5.3]) can be used at the expense of $O(m)$ arithmetic operations only to solve (34).

Although Eq. (34) is theoretically correct, numerically it is feasible only in the case when all channels have positive energies, that is, when $p = s$. A scaling procedure for negative channels will now be described. The corresponding numerical algorithm will be presented in Subsection 4.1. Suppose that channel l is a negative energy channel. Then the lth component of Y_i is of the size of $\exp(k_l b_i)$ which can be very large for i close to m,

while the lth component of Z_i becomes very small, of the size of $\exp(-k_l b_i)$. In order to balance the size of computed quantities, the following scaling is introduced in negative energy channels. Let E_i denote the scaling diagonal matrices

$$E_i = \operatorname{diag}(1, \ldots, 1, \exp(-k_{s+1} b_i), \ldots, \exp(-k_p b_i)), \qquad i = 1, \ldots, m,$$

and redefine

$$y_i = Y_i E_i, \qquad z_i = Z_i E_i^{-1}, \qquad a_i = E_i^{-1} A_i, \qquad b_i = E_i B_i,$$

with the result that in the ith subinterval Eq. (25) now reads

$$\Psi_j = y_i a_i + z_i b_i.$$

Next introduce the global $2mp \times 2mp$ scaling diagonal matrix

$$E = \operatorname{diag}\big(E_1, \ldots, E_m, E_1^{-1}, \ldots, E_m^{-1}\big)$$

and the scaled versions of $S(r)$ and $C(r)$,

$$c(r) = E_i^{-1} C(r), \qquad s(r) = E_i S(r), \quad r \in [b_{i-1}, b_i].$$

With this notation in place, the local equations (21) and (22) become

$$\begin{aligned} y_i(r) + K^{-1} s(r) \int_r^{b_i} c(r') V(r') y_i(r')\, dr' + K^{-1} c(r) \int_{b_{i-1}}^{r} s(r') V(r') y_i(r')\, dr' \\ = s(r), \qquad b_{i-1} \le r \le b_i, \end{aligned} \tag{35}$$

and

$$\begin{aligned} z_i(r) + K^{-1} s(r) \int_r^{b_i} c(r') V(r') z_i(r')\, dr' + K^{-1} c(r) \int_{b_{i-1}}^{r} s(r') V(r') z_i(r')\, dr' \\ = c(r), \qquad b_{i-1} \le r \le b_i. \end{aligned} \tag{36}$$

Note that the matrices E, S, C, and K^{-1} are all diagonal and therefore commute with each other. Also note that the entries in c and s, and hence in y_i and z_i, are now of an ordinary size.

The inner products (27), (28), (30), and (31) are changed exactly in the same way, with C, S, Y_q, and Z_q replaced by the corresponding lower case. Equation (33) can be rewritten as

$$E^{-1} \mathcal{L} E E^{-1} A = E^{-1} F,$$

or in more detail,

$$\begin{pmatrix} \lambda_{11} & \lambda_{12} \\ \lambda_{21} & \lambda_{22} \end{pmatrix} \begin{pmatrix} a_1 \\ a_2 \\ \vdots \\ a_m \\ b_1 \\ b_2 \\ \vdots \\ b_m \end{pmatrix} = \begin{pmatrix} 0 \\ 0 \\ \vdots \\ 0 \\ e_j \\ 0 \\ 0 \\ \vdots \\ 0 \end{pmatrix},$$

where

$$\lambda_{11} = \begin{pmatrix} I & E_1^{-1}E_2(cy_2 - I) & & & 0 \\ & I & E_2^{-1}E_3(cy_3 - I) & & \\ & & I & \ddots & \\ & & & \ddots & E_{m-1}^{-1}E_m(cy_m - I) \\ 0 & & & & I \end{pmatrix},$$

$$\lambda_{12} = \begin{pmatrix} 0 & E_1^{-1}E_2(cz_2) & & & 0 \\ & 0 & E_2^{-1}E_3(cz_3) & & \\ & & 0 & \ddots & \\ & & & \ddots & E_{m-1}^{-1}E_m(cz_m) \\ 0 & & & & 0 \end{pmatrix},$$

$$\lambda_{21} = \begin{pmatrix} 0 & & & & 0 \\ E_2E_1^{-1}(sy_1) & \ddots & & & \\ & \ddots & 0 & & \\ & & E_{m-2}E_{m-3}^{-1}(sy_{m-2}) & 0 & \\ 0 & & & E_{m-1}E_{m-2}^{-1}(sy_{m-1}) & 0. \end{pmatrix},$$

and

$$\lambda_{22} = \begin{pmatrix} I & & & & 0 \\ E_2E_1^{-1}(sz_1 - I) & \ddots & & & \\ & \ddots & I & & \\ & & E_{m-2}E_{m-3}^{-1}(sz_{m-2} - I) & I & \\ 0 & & & E_{m-1}E_{m-2}^{-1}(sz_{m-1} - I) & I \end{pmatrix}.$$

Note that the entries in $E_i^{-1}E_{i+1}$ and $E_iE_{i-1}^{-1}$ are also of an ordinary size. Again changing order of variables we transform it into a banded block tridiagonal system

$$\begin{pmatrix} \mathbf{I} & \mathbf{m}_{12} & & & 0 \\ \mathbf{m}_{21} & \mathbf{I} & \mathbf{m}_{23} & & \\ & \mathbf{m}_{32} & \ddots & \ddots & \\ & & \ddots & \mathbf{I} & \mathbf{m}_{m-1,m} \\ 0 & & & \mathbf{m}_{m,m-1} & \mathbf{I} \end{pmatrix} \begin{pmatrix} a_1 \\ b_1 \\ a_2 \\ b_2 \\ \vdots \\ a_m \\ b_m \end{pmatrix} = \begin{pmatrix} 0 \\ 0 \\ \vdots \\ 0 \\ e_j \\ 0 \end{pmatrix}, \tag{37}$$

where

$$\mathbf{m}_{i-1,i} = \begin{pmatrix} cy_i - I & cz_i \\ 0 & 0 \end{pmatrix}, \qquad i = 2, \ldots, m,$$

and

$$\mathbf{m}_{i,i-1} = \begin{pmatrix} 0 & 0 \\ sy_{i-1} & sz_{i-1} - I \end{pmatrix}, \qquad i = 2, \ldots m.$$

4. DISCRETIZATION OF LOCAL EQUATIONS

Although the discretization procedure described below is similar to the one in [1], but because of the added notational complexity, we repeat the main steps of this discretization for the reader's convenience.

In this section we describe the numerical technique for discretizing the local equations (21) and (22), which is a generalization to the multi-channel case of Section 4 in [1]. It is based on the Clenshaw–Curtis quadrature which is well suited for computing anti-derivatives and hence for discretizing integrals present in (21) and (22). Assume $f(r)$ is a function given in the interval $[-1, 1]$ and define

$$F(r) = \int_{-1}^{r} f(r')\, dr', \qquad -1 \le r \le 1.$$

Further, assume that $f(r)$ can be expanded in a finite set of Chebyshev polynomials, i.e.,

$$f(r) = \sum_{j=0}^{n} \alpha_j T_j(r), \qquad -1 \le r \le 1, \tag{38}$$

where

$$T_j(r) = \cos(j \arccos(r)), \qquad j = 0, 1, \ldots, n,$$

are the Chebyshev polynomials. Clenshaw and Curtis [8] showed that if

$$F(r) = \sum_{j=0}^{n+1} \beta_j T_j(r),$$

then

$$[\beta_0, \beta_1, \ldots, \beta_n]^T = \mathbf{S}_L[\alpha_0, \alpha_1, \ldots, \alpha_n]^T,$$

where

$$\mathbf{S}_L = \begin{pmatrix} 1 & 1 & -1 & 1 & \cdots & (-1)^{(n+1)} \\ & 1 & & & & 0 \\ & & 1 & & & \\ & & & 1 & & \\ & & & & \ddots & \\ 0 & & & & & 1 \end{pmatrix} \begin{pmatrix} 0 & & & & & 0 \\ 1 & 0 & -\frac{1}{2} & & & \\ & \frac{1}{4} & 0 & -\frac{1}{4} & & \\ & & \frac{1}{6} & \ddots & \ddots & \\ & & & \ddots & 0 & -\frac{1}{2(n-1)} \\ 0 & & & & \frac{1}{2n} & 0 \end{pmatrix}$$

is the so-called left spectral integration matrix. Here $[\nu]^T$ denotes the transpose of the column vector ν. Similarly, if

$$\tilde{F}(r) = \int_r^1 f(r')\,dr' = \sum_{j=0}^{n+1} \tilde{\beta}_j T_j(r),$$

then

$$[\tilde{\beta}_0, \tilde{\beta}_1, \ldots, \tilde{\beta}_n]^T = \mathbf{S}_R[\alpha_0, \alpha_1, \ldots, \alpha_n]^T,$$

where the right spectral integration matrix is given by

$$\mathbf{S}_R = \begin{pmatrix} 1 & & & \cdots & 1 \\ & -1 & & & 0 \\ & & -1 & & \\ & & & \ddots & \\ 0 & & & & -1 \end{pmatrix} \begin{pmatrix} 0 & & & & & 0 \\ 1 & 0 & -\frac{1}{2} & & & \\ & \frac{1}{4} & 0 & -\frac{1}{4} & & \\ & & \frac{1}{6} & \ddots & \ddots & \\ & & & \ddots & 0 & -\frac{1}{2(n-1)} \\ 0 & & & & \frac{1}{2n} & 0 \end{pmatrix}.$$

Since $T_j(1) = 1$ for all j, we also have that

$$F(1) = \int_{-1}^1 f(r')\,dr' = \sum_{j=0}^{n+1} \beta_j. \tag{39}$$

Using (38) one can find the Chebyshev–Fourier coefficients, α_j, of $f(r)$ as follows. Let τ_k, $k = 0, \ldots, n$, denote the zeros of T_{n+1} viz.,

$$\tau_k = \cos\frac{(2k+1)\pi}{2(n+1)},$$

so that

$$T_j(\tau_k) = \cos\frac{(2k+1)j\pi}{2(n+1)}, \qquad k, j = 0, \ldots, n.$$

Substituting $r = \tau_k$, $k = 0, \ldots, n$, into (38), we obtain that

$$\begin{bmatrix} f(\tau_0) \\ \vdots \\ f(\tau_n) \end{bmatrix} = \mathbf{C} \begin{bmatrix} \alpha_0 \\ \vdots \\ \alpha_n \end{bmatrix},$$

where $\mathbf{C}$ is a discrete cosine transform matrix whose elements are specified by

$$\mathbf{C}_{kj} = T_j(\tau_k), \qquad k, j = 0, \ldots, n.$$

The matrix $\mathbf{C}$ has orthogonal columns, that is,

$$\mathbf{C}^T\mathbf{C} = \operatorname{diag}\left(n, \frac{n}{2}, \ldots, \frac{n}{2}\right).$$

Therefore,

$$\mathbf{C}^{-1} = \operatorname{diag}\left(\frac{1}{n}, \frac{2}{n}, \ldots, \frac{2}{n}\right)\mathbf{C}^T.$$

Moreover, the matrix $\mathbf{C}$ (as well as $\mathbf{C}^T$ and $\mathbf{C}^{-1}$) can be applied to a vector at the cost of $O(n \log n)$ arithmetic operations. These and other properties of discrete cosine transforms can be found in C. Van Loan [13]. Thus the vector

$$[\alpha_0, \alpha_1, \ldots, \alpha_n]^T = \mathbf{C}^{-1}[f(\tau_0),\ f(\tau_1), \ldots,\ f(\tau_n)]^T$$

can be easily found from values of f at $\tau_0, \ldots, \tau_n$. In particular,

$$\begin{bmatrix} F(\tau_0) \\ \vdots \\ F(\tau_n) \end{bmatrix} = \mathbf{C}\mathbf{S}_L\mathbf{C}^{-1} \begin{bmatrix} f(\tau_0) \\ \vdots \\ f(\tau_n) \end{bmatrix} \tag{40}$$

and, similarly,

$$\begin{bmatrix} \tilde{F}(\tau_0) \\ \vdots \\ \tilde{F}(\tau_n) \end{bmatrix} = \mathbf{C}\mathbf{S}_R\mathbf{C}^{-1} \begin{bmatrix} f(\tau_0) \\ \vdots \\ f(\tau_n) \end{bmatrix}. \tag{41}$$

We remark that in writing the equality sign in (40) and (41), we assume that β_{n+1} is set to zero. This is an acceptable assumption because $f(r)$ is itself only approximately represented by the polynomial in (38) and the overall accuracy of approximation is not affected.

The formulas (40) and (41) can be generalized for intervals $[b_{i-1}, b_i]$ other than $[-1, 1]$ by the linear change of variable

$$h_i(t) = \frac{1}{2}(b_i - b_{i-1})t + \frac{1}{2}(b_i + b_{i-1}).$$

Thus if

$$\tau_j^{(i)} = h_i(\tau_j), \qquad j = 0, \ldots, n$$

then

$$\begin{bmatrix} F(\tau_0^{(i)}) \\ \vdots \\ F(\tau_n^{(i)}) \end{bmatrix} = \frac{(b_i - b_{i-1})}{2} \mathbf{C}\mathbf{S}_L\mathbf{C}^{-1} \begin{bmatrix} f(\tau_0^{(i)}) \\ \vdots \\ f(\tau_n^{(i)}) \end{bmatrix} \tag{42}$$

and, similarly,

$$\begin{bmatrix} \tilde{F}(\tau_0^{(i)}) \\ \vdots \\ \tilde{F}(\tau_n^{(i)}) \end{bmatrix} = \frac{(b_i - b_{i-1})}{2} \mathbf{C}\mathbf{S}_R\mathbf{C}^{-1} \begin{bmatrix} f(\tau_0^{(i)}) \\ \vdots \\ f(\tau_n^{(i)}) \end{bmatrix}. \tag{43}$$

Using (40) and (41) we can now discretize the local equations (21) and (22) as follows. Let $\mathbf{J}$ denote the $(n+1)p \times (n+1)p$ permutation matrix which transforms a vector

$$(a_{11}, \ldots, a_{p1}, a_{12}, \ldots, a_{p2}, \ldots, a_{1m}, \ldots, a_{p,n+1})^T$$

into the vector

$$(a_{11}, a_{12}, \ldots, a_{1,n+1}, a_{21}, a_{22}, \ldots, a_{2,n+1}, a_{p1}, a_{p2}, \ldots, a_{p,n+1})^T.$$

Let us also denote

$$\mathbf{Y}_i = \begin{bmatrix} Y_i(\tau_0^{(i)}) \\ \vdots \\ Y_i(\tau_n^{(i)}) \end{bmatrix}, \qquad \mathbf{S}_i = \begin{bmatrix} S(\tau_0^{(i)}) \\ \vdots \\ S(\tau_n^{(i)}) \end{bmatrix},$$

and similarly $\mathbf{Z}_i$ and $\mathbf{C}_i$.

Let us also introduce the following block diagonal matrices with $n+1$ blocks of the same size, $p \times p$,

$$\begin{aligned} \mathbf{Q}_L &= \operatorname{diag}\big(\mathbf{C}\mathbf{S}_L\mathbf{C}^{-1}, \ldots, \mathbf{C}\mathbf{S}_L\mathbf{C}^{-1}\big), \\ \mathbf{Q}_R &= \operatorname{diag}\big(\mathbf{C}\mathbf{S}_R\mathbf{C}^{-1}, \ldots, \mathbf{C}\mathbf{S}_R\mathbf{C}^{-1}\big), \\ \mathbf{D}_{S_i} &= \operatorname{diag}\big(S(\tau_0^{(i)}), \ldots, S(\tau_n^{(i)})\big), \end{aligned}$$

and similarly, $\mathbf{D}_{C_i}$, $\mathbf{D}_{CV_i}$, $\mathbf{D}_{SV_i}$, and finally $K^{-1} = \operatorname{diag}(K^{-1}, \ldots, K^{-1})$.

In particular, the product $\mathbf{J}\mathbf{D}_{SV_i}\mathbf{Y}_i$ rearranges the entries of $\mathbf{D}_{SV_i}\mathbf{Y}_i$ in such a way that block by block application of $\mathbf{C}\mathbf{S}_L C^{-1}$ transforms the values of $\mathbf{D}_{SV_i}\mathbf{Y}_i$ into values of its

anti-derivative, which are returned to the original ordering by the application of $\mathbf{J}^T$. With this notation in place we can discretize now (21) as

$$\left(\mathbf{I}+\frac{(b_i-b_{i-1})}{2}\mathbf{K}^{-1}\left(\mathbf{D}_{S_i}\mathbf{J}^T\mathbf{Q}_R\mathbf{J}\mathbf{D}_{CV_i}+\mathbf{D}_{C_i}\mathbf{J}^T\mathbf{Q}_L\mathbf{J}\mathbf{D}_{SV_i}\right)\right)\mathbf{Y}_i=\mathbf{S}_i, \tag{44}$$

and similarly for (22) we have

$$\left(\mathbf{I}+\frac{(b_i-b_{i-1})}{2}\mathbf{K}^{-1}\left(\mathbf{D}_{S_i}\mathbf{J}^T\mathbf{Q}_R\mathbf{J}\mathbf{D}_{CV_i}+\mathbf{D}_{C_i}\mathbf{J}^T\mathbf{Q}_L\mathbf{J}\mathbf{D}_{SV_i}\right)\right)\mathbf{Z}_i=\mathbf{C}_i, \tag{45}$$

where $\mathbf{I}$ is the identity matrix of an appropriate size. The solution of (44) and (45) can be done using standard software, e.g., Gaussian elimination with partial pivoting at the cost of $O(n^3)$ arithmetic operations. The solutions $\mathbf{Y}_i$ and $\mathbf{Z}_i$ give approximate values to the local functions $Y_i(r)$ and $Z_i(r)$ at the Chebyshev nodes in each of the subintervals $[b_{i-1}, b_i]$, $i=1,\ldots,m$. The inner products (27), (28), (30), and (31) can now be obtained using (39) as follows. Let

$$\mathbf{R}_L=\operatorname{diag}\left(\mathbf{S}_L\mathbf{C}^{-1},\ldots,\mathbf{S}_L\mathbf{C}^{-1}\right),$$

then

$$\begin{aligned}
(CY_i)&=\frac{b_i-b_{i-1}}{2}K^{-1}[1_1,1_2,\ldots,1_p]\mathbf{R}_L\mathbf{J}\mathbf{D}_{CV_i}\mathbf{Y}_i,\\
(CZ_i)&=\frac{b_i-b_{i-1}}{2}K^{-1}[1_1,1_2,\ldots,1_p]\mathbf{R}_L\mathbf{J}\mathbf{D}_{CV_i}\mathbf{Z}_i,\\
(SY_i)&=\frac{b_i-b_{i-1}}{2}K^{-1}[1_1,1_2,\ldots,1_p]\mathbf{R}_L\mathbf{J}\mathbf{D}_{SV_i}\mathbf{Y}_i,\\
(SZ_i)&=\frac{b_i-b_{i-1}}{2}K^{-1}[1_1,1_2,\ldots,1_p]\mathbf{R}_L\mathbf{J}\mathbf{D}_{SV_i}\mathbf{Z}_i,
\end{aligned}$$

where 1_k is a $p\times(n+1)$ matrix whose row number k equals $[1,\ldots,1]$, while the rest are zeros. The solution of the scaled problem is computed in very much the same way.

The computation of each of the above inner products takes $O(p(n+1))$ arithmetic operations after $[1_1,1_2,\ldots,l_p]\mathbf{R}_L$ is precomputed at the cost of $O((n+1)^3)$ flops and is negligible relative to the cost of solving (44) and (45). These inner products are substituted into (34) and the weights A_i, B_i are obtained at the cost of $O(pm)$ arithmetic operations. The coefficient in $O(m)$ is of order unity and hence much smaller than $(p(n+1))^3$ in $O((p(n+1))^3m)$ needed to compute $\mathbf{Y}_i,\mathbf{Z}_i$, $i=1,\ldots,m$. Thus the overall cost of the computation is dominated by the $O((p(n+1))^3m)$ cost of solving local equations (44) and (45). The cost of solving local equations can be reduced by the use of parallel processors since the calculation of $\mathbf{Y}_i$ and $\mathbf{Z}_i$ on each subinterval is independent.

Using the sparseness of $\mathbf{S}_L$ and $\mathbf{S}_R$ and the fast implementation of the discrete cosine transform, one may also try to reduce the cost of solving (44) and (45) by the use of iterative algorithms.

After A_i and B_i are found we finally obtain

$$\begin{bmatrix}\Psi_j\left(\tau_0^{(i)}\right)\\ \vdots\\ \Psi_j\left(\tau_n^{(i)}\right)\end{bmatrix}\approx\mathbf{Y}_iA_i+\mathbf{Z}_iB_i.$$

To estimate the accuracy of approximation, we use the following property of Chebyshev expansions:

PROPOSITION 2. *Let* $f \in C^p[-1, 1]$, $p > 1$, *and*

$$f(r) = \sum_{j=0}^{\infty} \alpha_j T_j(r), \qquad -1 \le r \le 1.$$

Then

$$|\alpha_j| \le \left\{ \frac{2}{\pi} \int_0^{\pi} \left| \frac{d^p}{d\theta^p} f(\cos\theta) \right| d\theta \right\} \frac{1}{j^p} = \frac{c}{j^p}$$

and

$$\left| f(r) - \sum_{j=0}^{n} \alpha_j T_j(r) \right| \le \frac{c}{p-1} \frac{1}{n^{p-1}}.$$

The proof of this proposition is outlined in [10, p. 29]. It implies that if $f(r)$ is analytic then the convergence of the Chebyshev expansion is super-linear.

Using this proposition, one can show, see [9], that for $i = 1, \ldots, m$,

$$\left\| \begin{bmatrix} \Psi_j\left(\tau_0^{(i)}\right) \\ \vdots \\ \Psi_j\left(\tau_n^{(i)}\right) \end{bmatrix} - (\mathbf{Y}_i A_i + \mathbf{Z}_i B_i) \right\|_{\infty} \le \frac{\mathcal{C}_p}{n^p},$$

where $\mathcal{C}_p$ is a constant which depends on p only, provided that $V(r)$ is continuously differentiable p times for $0 < r < \infty$.

This spectral type high accuracy of approximation of Ψ_j with $\mathbf{Y}_i A_i + \mathbf{Z}_i B_i$, for modest values of n, was illustrated for the uncoupled channel case in [1], and will be further illustrated with numerical examples in the next section. The high accuracy of approximation here is due to the special feature of Clenshaw–Curtis quadrature: the highly accurate computation of the antiderivative. Since the kernel of the integral equations (21) and (22) is not smooth across the diagonal $\{r = r'\}$, the standard Nystrom type discretization methods will fail to give high accuracy in this case (see, e.g., L. M. Delves and J. L. Mohamed [14]).

Finally, we remark that the values of Ψ_j are found inside each of the subintervals of partition at Chebyshev nodes $\tau_0^{(i)}, \ldots, \tau_n^{(i)}$. The value of Ψ_j at T (or any other point in $[0, T]$, for that matter) can be found as follows. Using $\mathbf{C}^{-1}$ we can find Chebyshev–Fourier coefficients in $[b_{i-1}, b_i]$,

$$\begin{bmatrix} \alpha_0^{(i)} \\ \vdots \\ \alpha_n^{(i)} \end{bmatrix} = \mathbf{C}^{-1} \begin{bmatrix} \Psi_j\left(\tau_0^{(i)}\right) \\ \vdots \\ \Psi_j\left(\tau_n^{(i)}\right) \end{bmatrix}.$$

Thus,

$$\Psi_j(r) = \sum_{k=0}^{n} \alpha_k^{(i)} T_k(h_i(r)), \qquad b_{i-1} \le r \le b_i.$$

The value of $\Psi_j(r)$ (or $\Psi_j'(r)$) for $r \ne \tau_l^{(i)}$ can be found using the recursion satisfied by

Chebyshev polynomials,

$$T_{k+1}(x) = 2xT_k(x) - T_{k-1}(x).$$

In fact, we have used a backward (numerically more reliable) recursion suggested in [8].

4.1. *The Scaled Algorithm*

Here we outline in a pseudocode our algorithm for the scaled version of local equations (35) and (36).

For $j = 1, \ldots, m$,
  For $i = 1, \ldots, s$,
    Solve discretizations of (35) and (36),

$$\left(\mathbf{I} + \frac{(b_i - b_{i-1})}{2}\mathbf{K}^{-1}\left(\mathbf{D}_{s_i}\mathbf{J}^T\mathbf{Q}_R\mathbf{J}\mathbf{D}_{cV_i} + \mathbf{D}_{c_i}\mathbf{J}^T\mathbf{Q}_L\mathbf{J}\mathbf{D}_{sV_i}\right)\right)\mathbf{Y}_i = \mathbf{s}_i,$$
$$\left(\mathbf{I} + \frac{(b_i - b_{i-1})}{2}\mathbf{K}^{-1}\left(\mathbf{D}_{s_i}\mathbf{J}^T\mathbf{Q}_R\mathbf{J}\mathbf{D}_{cV_i} + \mathbf{D}_{c_i}\mathbf{J}^T\mathbf{Q}_L\mathbf{J}\mathbf{D}_{sV_i}\right)\right)\mathbf{Z}_i = \mathbf{c}_i,$$

    Compute

$$(cy_i) = \frac{b_i - b_{i-1}}{2}K^{-1}[1_1, 1_2, \ldots, 1_p]\mathbf{R}_L\mathbf{J}\mathbf{D}_{cV_i}\mathbf{y}_i,$$
$$(cz_i) = \frac{b_i - b_{i-1}}{2}K^{-1}[1_1, 1_2, \ldots, 1_p]\mathbf{R}_L\mathbf{J}\mathbf{D}_{cV_i}\mathbf{z}_i,$$
$$(sy_i) = \frac{b_i - b_{i-1}}{2}K^{-1}[1_1, 1_2, \ldots, 1_p]\mathbf{R}_L\mathbf{J}\mathbf{D}_{sV_i}\mathbf{y}_i,$$
$$(sz_i) = \frac{b_i - b_{i-1}}{2}K^{-1}[1_1, 1_2, \ldots, 1_p]\mathbf{R}_L\mathbf{J}\mathbf{D}_{sV_i}\mathbf{z}_i,$$

  Endfor
  Form and solve the linear system of equations (37).
  Compute Chebyshev coefficients of the components of the solution Ψ_j in the last subinterval of partition,

$$x_j = diag(C^{-1}, \ldots, C^{-1})\mathbf{J}(y_m a_m + z_m b_m).$$

  For $i = 1, \ldots, s$,
    use the Chebyshev coefficients of the ith component of Ψ_j, namely,

$$x_j((i-1)n + i : in + i)$$

    to compute $\Psi_{ij}(T)$ and $\Psi'_{ij}(T)$ using the above three-term recursion satisfied by Chebyshev polynomials and their derivatives and compute α_{ij} and β_{ij} via (16) and (17).
  Endfor
  Solve (20).
Endfor.

5. NUMERICAL EXAMPLES

The first two examples are used for numerical testing of the IEM. They contain exponential potentials for which analytical solutions are known in some cases and are not intended

to represent real life physical situations. A more realistic Lennard–Jones potential with constants corresponding to a real case is used as a third example.

The exponential potential matrix is of the form

$$V(r) = \begin{pmatrix} v_1 & u \\ u & v_2 \end{pmatrix} V_0 \exp(-r/\alpha), \tag{46}$$

and the values of V_0, α, v_1, v_2, u, and of the wave number k are specified in the numerical applications below. In the first example both channels have positive energies of equal value k^2. In the second example one channel has a positive energy k^2, and the other channel a negative energy $-k^2$. In the first example the analytic solution can be found, in the second example an analytic solution is not known to the authors. In the first two examples our numerical IEM is compared with a finite difference method, so as to obtain a comparison of accuracy of both methods. The finite difference method used is the Numerov algorithm [15], which was also used in our single channel paper [1], along with a variable step size method of Raptis and Cash, for numerical comparisons. We would like to emphasize once more that the purpose of the numerical experiments in this paper is mainly to illustrate the new features characteristic to coupled as opposed to single channel equations, rather than comparing the accuracy of numerical methods, which was already done in [1]. We choose here the Numerov method as a generic finite difference method because it is an easy to implement, reliable, and widely used method, although we are now aware of more advanced finite difference methods such as the recently developed exponentially fitted methods, see [16, 17] and references therein. A numerical comparison of our method with a finite element method and a Numerov-type finite difference method for the case of the Lennard–Jones potential can be found in [18].

In particular, we observe in the first example, in Subsection 5.1 below, that regardless of which finite difference method is used for solving initial value problems, the matching matrix for combining these solutions to satisfy the required asymptotic conditions can become increasingly ill conditioned. The IEM method does not have this potential disadvantage, as will be shown. We also observe in the second example of mixed positive-negative energy channels that the combination of outgoing and incoming solutions of initial value problems in finite difference methods needed to suppress growing solutions becomes quite cumbersome with an increasing number of channels. The IEM requires certain scaling of negative channels as described in Section 2, but there is no difficulty in combining the particular solutions to satisfy the required asymptotics.

5.1. *Two Positive Channel Energies*

The solution of the coupled equations is defined such that the asymptotic form of the upper and lower components is

$$\Psi \equiv \begin{pmatrix} \psi_1 \\ \psi_2 \end{pmatrix} \sim \begin{pmatrix} F_1(k_1 r) + \rho_1 G_1(k_1 r) \\ \rho_2 G_2(k_2 r) \end{pmatrix}, \tag{47}$$

where the functions F_i and G_i are the regular and irregular Riccati–Bessel functions $z_i j_{l_i}(z_i)$ and $-z_i y_{l_i}(z_i)$, respectively, and $z_i = k_i r$ for $i = 1, 2$. For the present case $k_1 = k_2 = k$ and $l_1 = l_2 = l$.

The procedure for obtaining the solution of the coupled equations by finite difference methods consists of constructing two functions ξ and π, whose upper and lower components

are zero at the origin, but which have different combinations of slopes at the origin,

$$\frac{d}{dr}\begin{pmatrix}\xi_1\\ \xi_2\end{pmatrix}_{r=0}=\begin{pmatrix}1\\ 0\end{pmatrix};\qquad \frac{d}{dr}\begin{pmatrix}\pi_1\\ \pi_2\end{pmatrix}_{r=0}=\begin{pmatrix}0\\ 1\end{pmatrix}. \tag{48}$$

The values of x and y for the appropriate linear combination of the two solutions

$$\Psi = x\,\Xi + y\,\Pi. \tag{49}$$

are obtained from the asymptotic requirement of (47). This is implemented by expressing the upper and lower components of the functions Ξ and Π in terms of the functions F_i and G_i

$$\xi_i = A_{i\xi}F_i + B_{i\xi}G_i;\qquad \pi_i = A_{i\pi}F_i + B_{i\pi}G_i,\ i=1,2, \tag{50}$$

in the vicinity of $r=T$, as is done near Eq. (16). For sufficiently large values of T, for which the non-centripetal potentials become negligible, the quantities A and B become constants. If the matrices $\mathcal{A}_F$ and $\mathcal{B}_F$ (F stands for the finite difference method) are defined as

$$\mathcal{A}_F=\begin{pmatrix}A_{1\xi} & A_{1\pi}\\ A_{2\xi} & A_{2\pi}\end{pmatrix}_{r=T};\qquad \mathcal{B}_F=\begin{pmatrix}B_{1\xi} & B_{1\pi}\\ B_{2\xi} & B_{2\pi}\end{pmatrix}_{r=T} \tag{51}$$

then x and y are obtained from

$$\mathcal{A}_F\begin{pmatrix}x\\ y\end{pmatrix}=\begin{pmatrix}1\\ 0\end{pmatrix}, \tag{52}$$

and ρ_1 and ρ_2 are obtained from

$$\begin{pmatrix}\rho_1\\ \rho_2\end{pmatrix}=\mathcal{B}_F\mathcal{A}_F^{-1}\begin{pmatrix}1\\ 0\end{pmatrix}. \tag{53}$$

Because the functions Ξ and Π are defined near the origin, then, under certain conditions they can become asymptotically nearly linearly dependent, regardless of the specific finite difference method used to solve (48). The more dependent they are, the more ill-conditioned the matrix $\mathcal{A}_F$ becomes, and the operation $\mathcal{A}_F^{-1}$ in (53) introduces correspondingly large errors, which add themselves to the intrinsic errors of the finite difference method. The former error can be assessed from the condition number of the matrix $\mathcal{A}_F$. For the exponential case with $l=0$ the functions Ξ, Π, the matrix $\mathcal{A}_F$, and its condition number can all be obtained analytically in terms of expressions involving Bessel functions and their derivatives. It is found that as the wave number k decreases toward zero the condition number increases exponentially as can be seen in Fig. 1. The effect becomes more pronounced as the range α of the exponential potential increases, as can be seen from Fig. 2.

By contrast the IEM method does not suffer from this difficulty. In the $l=0$ case it automatically produces the correct asymptotic behavior in both channels, without requiring the linear combination of two solutions. For $l\neq 0$ two solutions and their appropriate linear combination are required. They are obtained by driving the solution of the integral equation (15) either by the vector $v_1=(\sin(k_1r),0)^T$ or $v_2=(0,\sin(k_2r))^T$. The solution Ψ is

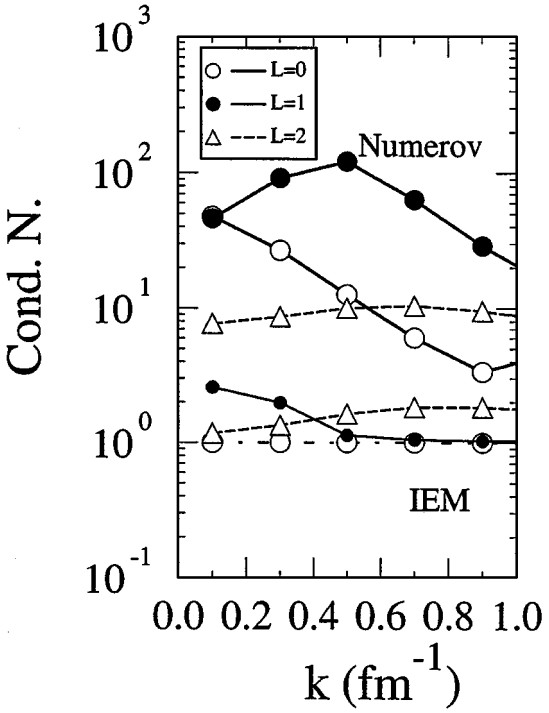

FIG. 1. The condition number of the matrix $\mathcal{A}$, defined in Eq. (51), as a function of the wave number k, for the two channel case with exponential potentials and positive energies. The range of the exponential potential defined in Eq. (46) is $\alpha = 1\ fm^{-1}$. The larger the condition number, the less independent the two solutions of the coupled equations become. The angular momentum number is denoted by L; the three lower curves are obtained with the integral equation method.

obtained from these two solutions as explained in Section 2 above, by means of Eq. (20). Our numerical examples confirm the well conditioning of the coefficient matrix in (20).

The condition number of a matrix is defined as the ratio of the largest to the smallest singular value of the matrix [11]. The singular values can be obtained numerically through the subroutine DLSVRR in the International Mathematical Scientific Library (IMSL.)

5.1.1. Numerical results. In this example the energies in both channels are equal and positive, and the potential strength is $V_0 = 5/\sqrt{2}\ fm^{-2}$ (the fm is the nuclear unit of length $=10^{-15}m$). The potential matrix, defined in (46), is taken to be of the form

$$\begin{pmatrix} v_1 & u \\ u & v_2 \end{pmatrix} = \begin{pmatrix} 1 & 1 \\ 1 & -1 \end{pmatrix}, \tag{54}$$

i.e., the diagonal potential in the incident channel is repulsive, in the second channel it is attractive, and the coupling potential is of the same strength. The values of the decay constant α will be either $1\ fm$ or $4\ fm$, and the corresponding values of the truncation radius T will be $50\ fm$ or $140\ fm$, respectively. The condition numbers for these two cases are shown in Figs. 1 and 2, as a function of the wave number $k_1 = k_2 = k$. The finite difference results are obtained with a coupled channel Numerov method which is accurate to the sixth order in the step-size h in each three-point interval (while the global accuracy is of order $\simeq h^{-4}$), and $h = 0.015625\ fm$. For the IEM the number of partitions, each with 16 Chebyshev points, for the two cases are 65 and 114, respectively. In the exponential examples the partitions

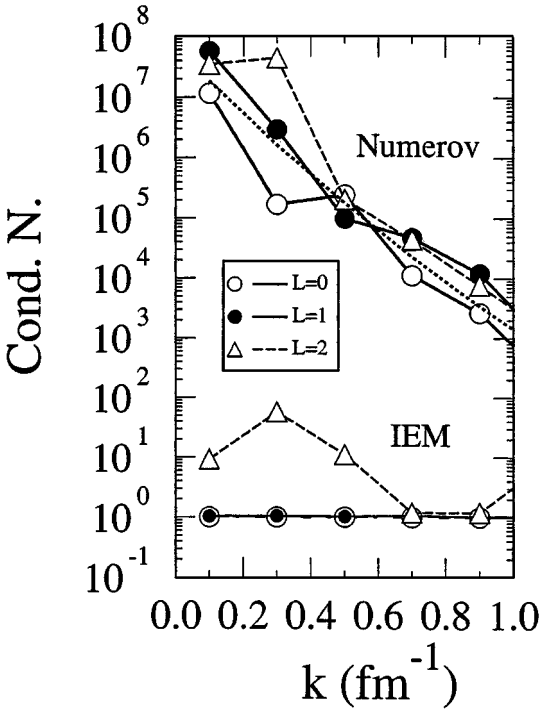

FIG. 2. Same as Fig. 1 for the case $\alpha = 4\ fm^{-1}$. The dotted line is obtained via an analytic simulation of the finite difference functions Ξ and Π, described in the text.

are equally spaced. The calculation is done on an IBM mainframe, in double precision with approximately 14 significant figures.

For the Numerov finite difference method the condition numbers of the matrix $\mathcal{A}_F$ for the $\alpha = 1$ case are less than about 100 for the three angular momentum numbers shown, indicating that no great loss of accuracy takes place in combining the two functions Ξ and Π in order to obtain Ψ. However, for the $\alpha = 4$ case the condition numbers become very large for small values of k, in agreement with the theoretical expectation, based on the analytic solutions, which for $l = 0$ is shown by means of the dotted line in Fig. 2. By contrast the condition numbers for the IEM case always remain small, less than approximately 100. The loss of accuracy for the Numerov case, and the lack of loss of accuracy for the IEM, expected from the values of the condition numbers of the matrix are analyzed in Fig. 3 for the $\alpha = 4, l = 0$ case. Shown are the absolute errors in the combined values of the asymptotic coefficients ρ_1 and ρ_2 as a function of the wave number. These errors are obtained by comparing the numerical values with the analytical ones. The IEM error (solid circles) is approximately one order of magnitude larger than the machine accuracy, while the Numerov errors are much larger and increase with decreasing values of k, as is expected from the condition numbers. A further demonstration that the condition numbers are responsible in large part for the lack of accuracy of the ρ values, rather than the error of the finite difference algorithm, is given by the two curves labeled Attr. and Rep. They represent the Numerov error of the ρ values for uncoupled cases, using either the attractive or the repulsive diagonal potential, respectively. This error is much lower than that for the coupled case, showing that the process of performing the linear combination of the two functions Ξ and Π introduces an additional substantial error.

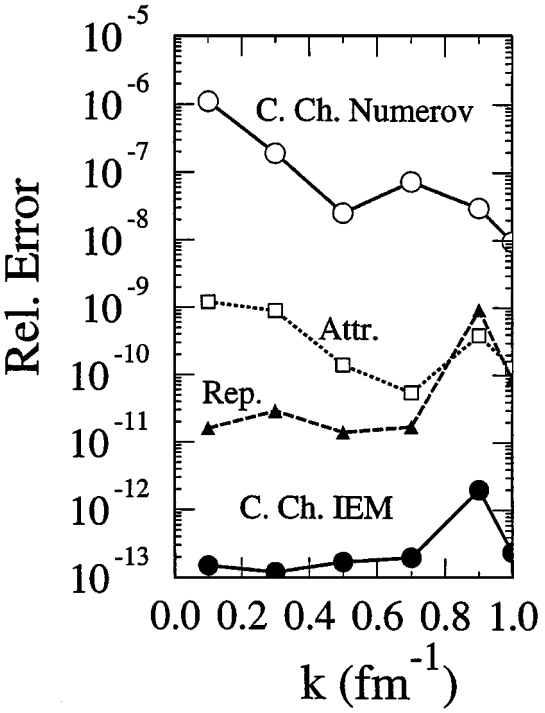

FIG. 3. Accuracy of the asymptotic constants ρ_1 and ρ_2 for the coupled channel case with exponential potentials and equal energies, as a function of the wave number k, for $l = 0$. The accuracy is obtained by comparison with the analytic results. The two middle lines, denoted Rep. and Attr., represent the accuracy of the Numerov method for the uncoupled cases, with a repulsive or attractive potential, respectively.

In Figs. 4 and 5 we examine in more detail the condition numbers for the IEM, $\alpha = 4$ case. It can be seen from Fig. 4 that among the various l-values examined, the values of the condition number are largest for $l = 2$ in the vicinity of $k = 0.3\ fm^{-1}$. A more detailed study shows that for k in the interval 0.28 to 0.31 fm^{-1} the determinant of the matrix A_{IEM} (the IEM equivalent of $\mathcal{A}_F$), goes through a zero, with a sharp discontinuity from $-\infty$ to $+\infty$ near $k = 0.30$. At this point the values of ρ_1 and ρ_2 also become infinite, which means that the phase shifts $\varphi_i = \arctan(\rho_i)$ go through a multiple of $\pi/2$. The occurrence of such points is inherent in the physical conditions of the problem at hand and is independent of the numerical method used for the evaluation of the corresponding coupled equations. For example, the condition numbers for the Numerov method are also large near the $l = 2, k = 0.3\ fm, \alpha = 4\ fm$ point.

In summary, the basic difference between the finite difference and the integral equation method in the solution of coupled equations lies in the linear independence of the solutions needed to satisfy the appropriate asymptotic boundary conditions. The solutions obtained by a finite difference method are maximally linearly independent near the origin, while the ones obtained from the IEM method maintain their linear independence asymptotically, because they are based on Greens functions which contain the appropriate asymptotic, behavior. This fact also holds for the coupling between channels some of which have negative energies, as will be demonstrated in the next section. In addition, the IEM, being a spectral method, has a higher inherent accuracy, than the finite difference methods.

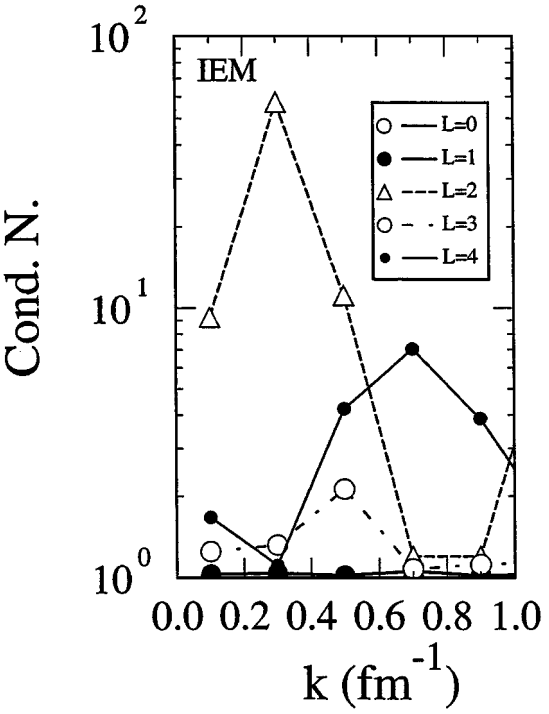

FIG. 4. Condition numbers for the IEM calculation for the coupled channel case described in Fig. 2, for five angular momentum numbers.

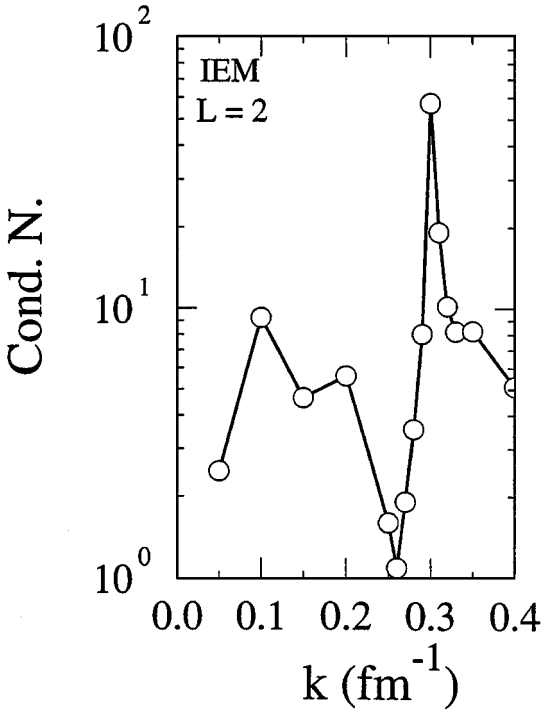

FIG. 5. Detail of the condition number for the case described in Fig. 4.

5.2. *One Positive and One Negative Channel Energy*

In this case the asymptotic behavior of the wave function will be described by the constants ρ_1 and ρ_2 according to

$$\Psi \equiv \begin{pmatrix} \psi_1 \\ \psi_2 \end{pmatrix} \sim \begin{pmatrix} F_1(kr) + \rho_1 G_1(kr) \\ \rho_2 \exp(-\kappa r) \end{pmatrix}, \tag{55}$$

where the functions F_i and G_i are defined in connection to (47).

This (pos-neg) case differs from the (pos-pos) energies case in three respects.

(a) The solution by the finite difference method is now more complicated because it requires the linear combination of five different functions: two "inside" solutions started near the origin and integrated outwards, as described in (48), and three "outside" solutions started at the truncation radius T and integrated inwards. At some intermediate distance these functions and their derivatives are matched to each other, leading to a 4×4 matrix for determining the appropriate linear combination of these functions. The fifth coefficient is determined from an overall asymptotic normalization. The three outside solutions have (upper, lower) components in the vicinity of $r = T$ of the form $(\sin kr, 0)$, $(\cos kr, 0)$, and $(0, \exp(-\kappa r))$, where k and κ are the wave numbers in the positive, respectively negative, energy channels. By contrast, as explained near Eq. (17), the IEM method requires only as many different solutions as there are positive energy channels (one solution in this two-channel example), because the exponentially decreasing character of the solutions in the negative energy channels is automatically implemented through the appropriate behavior of the respective Green's functions.

(b) The solution for the IEM is now also more complicated in that the Green's functions in each partition for the negative energy channel need to be scaled, as explained in Section 3 above, so as to compensate for the large disparity of their values. The Green's functions now include expressions $\sinh(\kappa r)$ and $\exp(-\kappa r)$, which for large values of r can have very different values from each other and from the Green's functions in the positive energy channel. Such scaling has been implemented successfully, as was tested by comparison with the analytic solution for an uncoupled negative energy channel with an exponential potential.

(c) The large-distance behavior of the negative energy wave function can be very sensitively affected by the coupling to the positive energy wave function, even though the coupling potential is small, but not zero. Thus, the asymptotic behavior $\exp(-\kappa r)$ is not achieved, and hence ρ_2 is T-dependent, unless the coupling potential is sufficiently small.

5.2.1. Numerical example. The features described above will now be illustrated by a numerical example with exponential potentials. The potential strength is again $V_0 = 5/\sqrt{2}\ fm^{-2}$, and the potential matrix, defined in (46) is of the form

$$\begin{pmatrix} v_1 & u \\ u & v_2 \end{pmatrix} = \begin{pmatrix} 1 & u \\ u & -1 \end{pmatrix}. \tag{56}$$

Unless stated otherwise, the coupling strength parameter u is equal to 1. Numerical evaluation of the asymptotic constants ρ_1 and ρ_2, for a fixed value of T and various choices of the partition number M, was found to be stable to 13 significant figures when $M \geq 40$, for both

TABLE I

Accuracy in ρ_1 and ρ_2, with the Numerov Method[a]

$k=\kappa$	$\alpha=1,\ T=25$		$\alpha=4,\ T=50$	
(fm^{-1})	(ρ_1, ρ_2)	$C.N.$[b]	(ρ_1, ρ_2)	$C.N.$[b]
0.25	(9, 8)	2.8(3)	(5, 3)	7.3(8)
0.50	(9, 8)	1.8(3)	(5, 3)	1.7(13)
0.75	(8, 6)	2.5(3)	(1, 2)	1.6(22)
1.00	(7, 5)	1.4(3)	(1, 0)	Overfl.
1.25	(8, 2)	4.5(3)	(0, 0)	Overfl.
1.50	(9, 2)	8.9(7)	(0, 0)	Overfl.

[a] The quantities (x, y) indicate the number of significant figures x and y for ρ_1 and ρ_2, respectively, which after rounding, agree with the IEM results.

[b] *C.N.* is the condition number, the figures in parentheses are the powers of 10 by which the preceding numbers are to be multiplied.

$\alpha=1\ fm$, and $\alpha=4\ fm$. An exception was the "resonance" case $k=0.25\ fm^{-1}$, $\alpha=4\ fm$, and $l=0$, for which ρ_1 was stable to only 10 significant figures. The accuracy of the solution obtained with the Numerov finite difference method was obtained by comparison with the IEM results. The smallest value of the step-size $h=2^{-7}\ fm$ employed tended to give the most accurate results. Table I shows that the Numerov method becomes increasingly inaccurate as the range α of the potential increases, and it fails completely for $\alpha=4\ fm$ and $\kappa>1$. The same is not the case with the IEM as is shown in Table II.

According to Tables I and II, the values of ρ_2 increase drastically as κ increases. The explanation can be found in the fact that the wave function in the negative energy channel does not decrease proportional to $\exp(-\kappa r)$, contrary to what is implied by (55), but it decreases proportional to the value of the coupling potential $\exp(-r/\alpha)$. This is the case whenever, in the negative energy channel, the coupling to the positive energy wave function dominates over the energy term, i.e., when $\kappa^2\psi_2 < V_{21}\psi_1$. This feature will now be illustrated by means of Figs. 6 and 7. The wave functions in the positive and negative energy channels, ψ_P and ψ_N, respectively, are illustrated in Fig. 6 for the case $l=0$, $k=\kappa=1.2\ fm^{-1}$,

TABLE II

Values of ρ_1 and ρ_2, Obtained with the IEM Method[a]

$k=\kappa$	$\alpha=1,\ T=25$		$\alpha=4,\ T=50$	
(fm^{-1})	ρ_1	ρ_2	ρ_1	ρ_2
0.25	−0.700811(0)	−0.274203(0)	−0.213745(2)	−0.188132(3)
0.50	−0.231030(1)	−0.747343(0)	0.267050(0)	0.145771(7)
0.75	0.268109(1)	−0.510719(1)	0.302913(0)	0.152607(12)
1.00	0.715728(−1)	−0.272947(1)	0.305707(1)	−0.543449(16)
1.25	−0.457558(0)	0.578646(3)	−0.335135(0)	0.482995(22)
1.50	−0.667470(0)	0.214832(6)	−0.499902(1)	0.202962(28)

[a] The figures in parentheses are the powers of 10 by which the preceding numbers are to be multiplied.

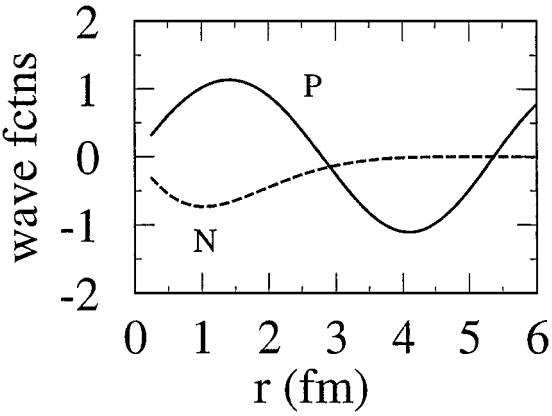

FIG. 6. Wave functions for the coupled channel case with one positive (P) and one negative (N) energy for $k = \kappa = 1.2\ fm^{-1}$. The exponential potential is described in Eqs. (46) and (54), with $\alpha = 1\ fm^{-1}$. The negative wave function is decaying to zero, as expected.

and $\alpha = 1\ fm$. It is clear that ψ_N decreases with the radial distance r. That the decrease is proportional to $\exp(-r/\alpha)$ can be seen from Fig. 7, which illustrates ψ_N multiplied by $\exp(r/\alpha)$ for $l = 0$ and 2 (solid lines). Even if the coupling potential is reduced by a factor of 100, the effect still persists, as is illustrated for $l = 0$ by the dashed line in Fig. 7. The oscillatory nature of ψ_N reflects the oscillatory nature of ψ_P.

5.3. *The Lennard–Jones Potential*

The purpose of this two channel example with one positive and one negative energy, respectively, is to demonstrate the performance of the IEM for a more realistic model calculation that captures the essence of the collision of two ultracold ^{2}S alkali atoms. It was suggested by E. Tiesinga and is examined in more detail in a further study [18].

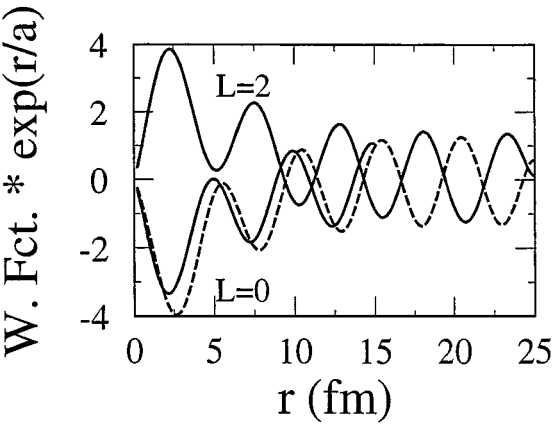

FIG. 7. Wave functions for the negative energy channel, for the case described in Fig. 6. In order to avoid having to use a logarithmic scale, the wave functions are multipled by $\exp(r/\alpha)$ times an appropriate constant. The oscillatory nature and the decay properties of the functions are due to the coupling to the positive energy channel. For the solid lines the coupling strength u in Eq. (54) is unity; for the dashed line it is $u = 0.01$.

The simplest multi-channel potential that describes the physics of the interaction between two colliding atoms is a two channel model. Taking into account that for small collision energies the nuclear rotation can be safely ignored, the non-rotating Hamiltonian is parametrized as

$$\left\{-\frac{\hbar^2}{2\mu}\mathbf{1}\frac{d^2}{dr^2}+\begin{pmatrix}\tilde{V}_{\rm LJ}(r) & \tilde{A}e^{-br}\\ \tilde{A}e^{-br} & \tilde{V}_{\rm LJ}(r)\end{pmatrix}-\begin{pmatrix}\tilde{E} & \\ & \tilde{E}-\tilde{E}_{\rm hf}\end{pmatrix}\right\}\begin{pmatrix}\psi_P\\ \psi_N\end{pmatrix}=0, \tag{57}$$

where the reduced mass $\mu = M/2$, $\tilde{E}_{\rm hf}$ is the asymptotic splitting energy between the two channels, and $\tilde{E}$ is the incident kinetic energy in the system. The r-dependent diagonal potentials of our test problem are of the Lennard–Jones form $\tilde{V}_{\rm LJ}(r) = \tilde{C}_{12}/r^{12} - \tilde{C}_6/r^6$ together with an off-diagonal exchange coupling given by $\tilde{A}e^{-br}$. The functions ψ_P and ψ_N describe the wavefunction for the open and closed channel, respectively.

For two colliding ultra-cold ^{2}S Na atoms, realistic values of the constants are [19] $M = 22.9897680$ amu, $\tilde{C}_6 = 1472$ a.u. $(a_0)^6$, $\tilde{C}_{12} = 38\times10^6$ a.u. $(a_0)^{12}$, $\tilde{A} = 2.9$ a.u., $b = 0.81173\ a_0$, and $\tilde{E}_{\rm hf} = 0.2693\times10^{-6}$ a.u. This choice of $\tilde{E}_{\rm hf}$ is approximately equal to the atomic hyperfine splitting of the ^{2}S Na atom. The total energy $\tilde{E} = 3.1668293\times10^{-12}$ a.u. corresponds to a temperature of 1 μK. Since $\tilde{E} \ll \tilde{E}_{\rm hf}$, the energy in the second channel is negative, i.e., only one of the two channels is asymptotically accessible. In the above a.u. stands for atomic units, and a_0 is the Bohr radius. The conversion into entirely a_0 units is achieved by multiplying the above equation by $2\mu/\hbar^2$. One obtains

$$\left(-\frac{d^2}{dr^2}+\mathcal{V}-\mathcal{E}\right)\begin{pmatrix}\psi_P\\ \psi_N\end{pmatrix}=0, \tag{58}$$

where r is in units of a_0 and the potential and energy matrices, $\mathcal{V}$ and $\mathcal{E}$, respectively, are in units of $(a_0)^{-2}$. The conversion of a quantity in a.u. units to $(a_0)^{-2}$ units is achieved by multiplying the former by $\mu = 22.989768\times1822.888506\,(\text{a.u.})^{-1}\,(a_0)^{-2}$. The potential matrix is

$$\mathcal{V}=\begin{vmatrix}V & U\\ U & V\end{vmatrix}, \tag{59}$$

where $V = \tilde{V}\times\mu$ and $U = \tilde{U}\times\mu$, and the energy matrix is

$$\mathcal{E}=\begin{vmatrix}k^2 & \\ & -\kappa^2\end{vmatrix}. \tag{60}$$

Here k and κ are the asymptotic wave numbers in each channel, given by $k = \sqrt{\tilde{E}\times\mu}$ and $\kappa = \sqrt{\tilde{E}_{\rm hf}\times\mu - k^2}$. The corresponding values are $k = 3.643004224146145\times10^{-4}\,(a_0)^{-1}$ and $\kappa = 0.1062338621818394\,(a_0)^{-1}$. The wave function is normalized so that asymptotically it becomes

$$\begin{pmatrix}\psi_P\\ \psi_N\end{pmatrix}\approx\begin{pmatrix}\sin(kr)+\rho_1\cos(kr)\\ \rho_2\exp(-\kappa r)\end{pmatrix}, \tag{61}$$

where ρ_1 and ρ_2 are two elements of the real scattering K matrix, in terms of which the phase shifts can be obtained.

Between 6 and 10 a_0 the diagonal potential is very deep leading to many oscillations in the wave functions, and at small distances the repulsive portion of the potential becomes

very large making the wave function very small. At large distances the wave functions change very slowly because of the small values of the asymptotic wave numbers. In order to accommodate such large variations in the local wave number, a variable partition size is introduced, as is described below. In order to allow for the singularity near the origin, a parameter R_{cut} is defined, and the wave functions are set to zero in the interval $[0, R_{cut}]$. A value of $R_{cut} = 4.0a_0$ is found to be satisfactory. In addition, the calculation is carried out to a maximum radius, $R_{\max}$, beyond which all potentials are set equal to zero. In the calculations displayed below, $R_{\max} = 500a_o$. At this distance the Lennard–Jones potential has the value $-3.95 \times 10^{-9} a_0^{-2}$. However, increasing the value of $R_{\max}$ has an effect beyond the 6th significant figure on the values of ρ_1 and ρ_2, as can be seen from the Table V. That such a small potential should have such a large effect on the phase-shift is due to the small energy. This is understandable in terms of perturbation theory, in which the integrals over the tail of the potential contain a factor $1/k$, which is large at small values of the energy.

In the version of the IEM method used for this section the (variable) size of each of the partitions is determined in terms of two parameters NL and ϵ as follows. In each radial region a local wave length in channels 1 and 2 is obtained as $2\pi/\sqrt{k^2 - V(r)}$, and $2\pi/\sqrt{|-\kappa^2 - V(r)|}$. The smaller of the two local wavelengths is taken, and the size of the partition in that region is determined such that there are a given total number NL of Chebyshev points per local wave length. Allowing for the fact that in each partition there are 16 Chebyshev points, the average length of a partition for a given local wave length λ is $\lambda \times 16/NL$. The length of each partition is subsequently readjusted using the tolerance parameter ϵ as follows. In each partition two sets of "local" functions are calculated in terms of which the global function ψ is obtained as a linear combination, as has been described before. The accuracy of each of the local functions can be determined by the size of the coefficients of the highest order Chebyshev polynomials. If the relative accuracy of the local functions in a given partition is larger than ϵ, then that partition is divided in half, and the testing is continued. If the initially chosen value of NL is too small, then the initial partitions are too large, and many of the partitions are subsequently reduced by the ϵ criterion. In this case the final number of partitions M becomes larger than their initial value. If the chosen value of NL is too large, then most of the partitions are unnecessarily small, and the value of M is too large, leading to a larger accumulation of roundoff errors for the final values of the K-matrix elements.

In summary, for a given value of ϵ, the value of NL was varied until the smallest number of partitions M was obtained. An example is given in Table III, for which $R_{\max}$ is set equal to $500a_o$.

From Table III one can find values of $\rho_1 = -0.3123339834$ and $\rho_2 = 6.576130397$ which are stable to ten significant figures. For values of the tolerance ϵ between 10^{-9} and 10^{-3} a good compromise value for $NL = 20$ was found. The values of M and the corresponding accuracy of ρ_1 are listed in Table IV for several values of ϵ.

The corresponding distribution of partitions for each of the three tolerance parameters is shown in Fig. 8. The increasingly large spacing of the partitions at the large distances is clear from the figure. In the vicinity of $R \simeq 50$ the density of partitions is high because the negative energy channel has a turning point there. This means that the local wave-length criterion alone would have been insufficient to determine the partition size.

An example of the variation of the ρ's with $R_{\max}$ is given in Table V, for which $\epsilon = 10^{-9}$.

TABLE III
Values of ρ_1, ρ_2, and Number of Partitions M as a Function of NL for the Tolerance $\epsilon = 10^{-9}$

NL	M	K_1	K_2
10	150	−0.31233398338182	6.5761303970458
20	153	−0.31233398338791	6.5761303971183
30	144	−0.31233398337104	6.5761303968390
40	154	−0.31233398338581	6.5761303970972
50	177	−0.31233398338729	6.5761303971378

TABLE IV
Accuracy for ρ_1 and Number of Partitions M for a Given Value of the Tolerance ϵ

ϵ	M	No. of sign. figs.
10^{-3}	30	5
10^{-6}	85	8
10^{-9}	153	10

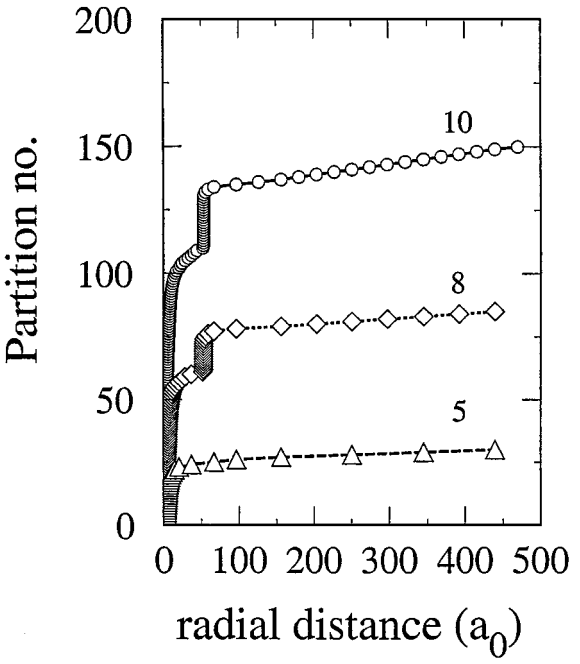

FIG. 8. Distribution of partition lengths for the Lennard–Jones cold atom collision example. This figure illusrates the results of Table IV. The points are located at the start of each partition with the corresponding partition number along the vertical axis. The circles, diamonds, and triangles correspond respectively to an accuracy parameter, ϵ, equal to 10^{-9}, 10^{-5}, and 10^{-3}. The corresponding number of significant figures of accuracy for the scattering quantity, ρ_1, is indicated next to each curve. The abrupt increase in the partition density near $r = 50a_o$ for the two upper curves is due to the local wave number in the negative channel going through zero near this point. The logarithmic derivative of the wave function changes sign in this region.

TABLE V
Dependence of ρ_1 and ρ_2 on $R_{\max}$

ρ_1	ρ_2	$R_{\max}$
−.313705209	6.62005410	250
−.312333983	6.57613040	500
−.312324588	6.57555968	1000
−.312324073	6.57558157	1500
−.312323719	6.57558741	2000

6. SUMMARY AND CONCLUSIONS

In this study we have extended the integral equation method of [1] to the case of coupled equations, in which at least one channel has a positive energy. The flexible partition structure of the one channel case is also preserved here, and so is the sparse nature of the "big" matrix required to obtain the coefficients A and B. These are the coefficients which, in each partition, combine the local solutions, Y and Z, into the global one. The high numerical accuracy is also maintained because the solutions in each partition are computed using a spectral type numerical method. The main difference to the uncoupled case is that for angular momentum numbers $\ell \neq 0$, the asymptotic boundary conditions are not as easy to satisfy for the positive energy channels as for the one-channel case. The coupled integral equations now have to be solved as many times as there are open channels, each time with a different driving term, and linear combinations between these solutions have to be implemented. However, in contrast to the solution of the coupled equations by a finite difference method, our IEM solutions are linearly independent at large distances, and the appropriate linear combinations can be obtained without difficulty. Further, the solutions in the negative energy channels automatically decay exponentially at large distances, because of the preestablished exponential behavior of the Green's functions. The "big" matrix M of the linear system of equations for the coefficients A and B is still block tridiagonal. The blocks, however, increase their dimension to twice the number of channels. For example, in the case of one channel, these block matrices are of dimension 2×2, for two channels they are 4×4, etc.

The accuracy properties were exhibited by means of numerical examples involving two channels. In one set of examples the potentials (diagonal and off-diagonal) were chosen to have the same exponential behavior but with different coefficients, because when the energies in both channels are equal and when $\ell = 0$ an analytical solution exists for comparison. The stability of the IEM method was generally to nine significant figures. Another numerical example for the case of the collision of two atoms at very low temperature, interacting with a long range Lennard–Jones potential was also carried out.

The differential equations can also be transformed into Volterra-type integral equations. The kernel of these equations is more singular at the origin than the kernel of the non-Volterra type, used in this and in our previous study. As is shown in the first part of the Appendix numerical calculations for various examples with the Volterra type show that this singularity does not affect the numerical accuracy, in fact, in all of our experiments the obtained accuracy was as good or better than that of the original IEM. In addition, the "big" matrix in this case is entirely lower triangular, and hence the solution for the coefficients A and B can be set up as a simple recursion which is more efficient and requires less

memory. The Volterra method is thus preferred, especially in the case of large scale systems of coupled equations. The description of this method is given in Appendix 1.

The IEM can be easily extended to the solution of an inhomogeneous second order differential equations. The presence of the inhomogeneous term $\mathcal{I}(r)$ requires minor modifications, and it does neither affect the partition structure nor the structure of the "Big" matrix M, which remains exactly the same as in the homogeneous case. A description of the method is presented for the uncoupled channel case in Appendix 2.

In summary, the coupled channel IEM method has good numerical stability and ease of implementation of the asymptotic boundary conditions for scattering situations. The method is carried out in configuration space, and hence is well suited for cases in which there are small effects which occur at large distances in the presence of many coupled channels, including the case where Coulomb potentials are present.

APPENDIXES

Here we present two relevant new developments in the single channel case. In the first one the Fredholm integral equation is replaced by a Volterra integral equation which leads to a block-triangular linear system of equations in (37), solved by a simple substitution. Apart from making the whole algorithm more efficient and accurate, it also simplifies substantially the corresponding FORTRAN code. For the sake of simplicity we give here only a brief outline of the Volterra formulation, and its extension to the multichannel case.

The second addition shows how to treat the inhomogeneous case.

APPENDIX 1: THE VOLTERRA FORMULATION

In the single channel case our integral equation formulation of the single channel Schrödinger equation is

$$\psi(r) + \frac{1}{k}\sin(kr)\int_r^T \cos(kr')V(r')\psi(r')\,dr' + \frac{1}{k}\cos(kr)\int_0^r \sin(kr')V(r')\psi(r')\,dr' = \sin(kr),$$

and can be rewritten as a Volterra equation as

$$\psi(r) + \frac{1}{k}\cos(kr)\int_0^r \sin(kr')V(r')\psi(r')\,dr' - \frac{1}{k}\sin(kr)\int_0^r \cos(kr')V(r')\psi(r')\,dr' = \left(1 - \frac{1}{k}\int_0^T \cos(kr')V(r')\psi(r')\,dr'\right)\sin(kr).$$

Therefore we can solve this equation instead and then scale its solution in the same way as before to match the required asymptotic behavior. Since the scaling of the right hand side is immaterial, we solve

$$\phi(r) + \frac{1}{k}\cos(kr)\int_0^r \sin(kr')V(r')\phi(r')\,dr' - \frac{1}{k}\sin(kr)\int_0^r \cos(kr')V(r')\phi(r')\,dr' = \sin(kr').$$

We now explain the few minor modifications required for the Volterra formulation and present results of our numerical experiments. After partitioning the interval $[0, T]$ into small subintervals, we solve in each subinterval a pair of equations,

$$y_i(r) + \frac{1}{k}\cos(kr)\int_{b_{i-1}}^{r} \sin(kr')V(r')y_i(r')\,dr' - \frac{1}{k}\sin(kr)\int_{b_{i-1}}^{r} \cos(kr')V(r')y_i(r')\,dr' = \sin(kr) \tag{62}$$

and

$$z_i(r) + \frac{1}{k}\cos(kr)\int_{b_{i-1}}^{r} \sin(kr')V(r')z_i(r')\,dr' - \frac{1}{k}\sin(kr)\int_{b_{i-1}}^{r} \cos(kr')V(r')z_i(r')\,dr' = \cos(kr), \tag{63}$$

such that the global solution, for r in the ith subinterval, is a linear combination of the local solutions,

$$\psi(r) = A_i y_i(r) + B_i z_i(r).$$

The coefficients A_i, B_i are found now from a simple recursion, rather than by solving a block-tridiagonal system of equations as in [1], $A_1 = 1$, $B_1 = 0$, and for $k = 2, \ldots, m$,

$$A_k = 1 + [(A_1 c y_1 + B_1 c z_1) + \cdots + (A_{k-1} c y_{k-1} + B_{k-1} c z_{k-1})],$$
$$B_{k-1} = -[(A_1 s y_1 + B_1 s z_1) + \cdots + (A_{k-1} s y_{k-1} + B_{k-1} s z_{k-1})],$$

with the notations exactly the same as in [1]. The derivation is very similar to the one in [1] and is omitted here. The discretization of the local equations (62) and (63) results in the following linear systems of equations,

$$\left[\mathbf{I} + \frac{b_i - b_{i-1}}{2k}\left(\mathbf{D}_{c_i}\mathbf{C}\mathbf{S}_L\mathbf{C}^{-1}\mathbf{D}_{s_i v_i} - \mathbf{D}_{s_i}\mathbf{C}\mathbf{S}_L\mathbf{C}^{-1}\mathbf{D}_{c_i v_i}\right)\right] y_i = s_i$$

and

$$\left[\mathbf{I} + \frac{b_i - b_{i-1}}{2k}\left(\mathbf{D}_{c_i}\mathbf{C}\mathbf{S}_L\mathbf{C}^{-1}\mathbf{D}_{s_i v_i} - \mathbf{D}_{s_i}\mathbf{C}\mathbf{S}_L\mathbf{C}^{-1}\mathbf{D}_{c_i v_i}\right)\right] z_i = c_i,$$

where the notation again is exactly the same as in [1].

To find the appropriate normalization constant we recall that for sufficiently large r the solution $\psi(r)$ is a linear combination of the corresponding Riccati–Bessel functions. So we chose $T_1 = T$ and T_2 near T and get

$$\psi(T_1) = \alpha F_l(T_1) + \beta G_l(T_1)$$
$$\psi(T_2) = \alpha F_l(T_2) + \beta G_l(T_2).$$

Therefore,

$$\begin{bmatrix} \alpha \\ \beta \end{bmatrix} = \begin{bmatrix} F_l(T_1) & G_l(T_1) \\ F_l(T_2) & G_l(T_2) \end{bmatrix}^{-1} \begin{bmatrix} \psi(T_1) \\ \psi(T_1), \end{bmatrix}$$

and the normalization constant is now given by

$$N_l = \frac{1}{\alpha - i\beta}.$$

Our numerical experiments show that this method is more efficient and more accurate than the original method based on the Fredholm formulation.

In the coupled channel case we replace the integral equation (5) with the corresponding Volterra integral equation,

$$\Psi_j(r) + K^{-1}C(r)\int_0^r S(r')V(r')\Psi_j(r')\,dr' - K^{-1}S(r)\int_0^r C(r')V(r')\Psi_j(r')\,dr' = U_j(r), \tag{64}$$

where the notations are the same as in the preceding sections. The restricted equations take the form

$$Y_i(r) + K^{-1}C(r)\int_{b_{i-1}}^r S(r')V(r')Y_i(r')\,dr' - K^{-1}S(r)\int_{b_{i-1}}^r C(r')V(r')Y_i(r')\,dr' = S(r) \tag{65}$$

and

$$Z_i(r) + K^{-1}C(r)\int_{b_{i-1}}^r S(r')V(r')Z_i(r')\,dr' - K^{-1}S(r)\int_{b_{i-1}}^r C(r')V(r')Z_i(r')\,dr' = C(r), \tag{66}$$

such that on the ith subinterval, $\Psi_j(r) = Y_k A_k + Z_k B_k$, where A_k and B_k are defined as before. The computation of A_k and B_k is much easier now, however, as they satisfy a simple recursion,

$$A_i = e_j - \sum_{k=1}^{i-1}[CY_kA_k + CZ_kB_k],$$

and

$$B_i = \sum_{k=1}^{i-1}[SY_kA_k + SZ_kB_k],$$

with $A_1 = e_j$ and $B_1 = 0$. The minor modification of the discretizations of the local equations is

$$\left(\mathbf{I} + \frac{(b_i - b_{i-1})}{2}\mathbf{K}^{-1}\left(\mathbf{D}_{C_i}\mathbf{J}^T\mathbf{Q}_L\mathbf{J}\mathbf{D}_{SV_i} - \mathbf{D}_{S_i}\mathbf{J}^T\mathbf{Q}_L\mathbf{J}\mathbf{D}_{CV_i}\right)\right)\mathbf{Y}_i = \mathbf{S}_i,$$

and

$$\left(\mathbf{I} + \frac{(b_i - b_{i-1})}{2}\mathbf{K}^{-1}\left(\mathbf{D}_{C_i}\mathbf{J}^T\mathbf{Q}_L\mathbf{J}\mathbf{D}_{SV_i} - \mathbf{D}_{S_i}\mathbf{J}^T\mathbf{Q}_L\mathbf{J}\mathbf{D}_{CV_i}\right)\right)\mathbf{Z}_i = \mathbf{C}_i.$$

To find the linear combination of $\Psi_1(r), \Psi_2(r), \ldots, \Psi_s(r)$ which satisfies the required asymptotics, we set $T_1 = T$, choose T_2 near T, and solve

$$\begin{bmatrix} \alpha_{ij} \\ \beta_{ij} \end{bmatrix} = \begin{bmatrix} F_{l_i}(T_1) & G_{l_i}(T_1) \\ F_{l_i}(T_2) & G_{l_i}(T_2) \end{bmatrix}^{-1} \begin{bmatrix} \Psi_{ij}(T_1) \\ \Psi_{ij}(T_2) \end{bmatrix}.$$

Then

$$R = x_1\Psi_1 + x_2\Psi_2 + \cdots + x_s\Psi_s,$$

where

$$\begin{bmatrix} x_1 \\ x_2 \\ \vdots \\ x_s \end{bmatrix} = \begin{bmatrix} \alpha_{11} & \alpha_{12} \cdots \alpha_{1s} \\ \alpha_{21} & \alpha_{22} \cdots \alpha_{2s} \\ & \vdots \\ \alpha_{s1} & \alpha_{s2} \cdots \alpha_{ss} \end{bmatrix}^{-1} \begin{bmatrix} 1 \\ 0 \\ \vdots \\ 0 \end{bmatrix}.$$

APPENDIX 2: SOLUTION OF THE INHOMOGENEOUS EQUATION

The equation to be solved is

$$\left(-\frac{d^2}{dr^2} + V_L(r) - k^2\right)\psi(r) = \mathcal{I}(r), \tag{67}$$

where V_L includes the centripetal potential and k is the wave number. Below we describe a method which avoids first having to calculate the distorted Green's function, but rather uses a procedure which is very similar to the one for solving the homogeneous equation.

We proceed by first writing the equation in the form

$$\left(\frac{d^2}{dr^2} + k^2\right)\psi(r) = V_L(r)\psi(r) - \mathcal{I}(r)$$

and then transforming it into the integral form

$$\psi(r) = \sin(kr) + \mathcal{G}_0 V_L \psi - \mathcal{G}_0 \mathcal{I}, \tag{68}$$

where $\mathcal{G}_0$ is the undistorted Green's function $(d^2/dr^2 + k^2)^{-1}$. Form this point on the procedure is very similar to that of the homogeneous case. One divides the radial range $[0, T]$ into m partitions $[b_{i-1}, b_i]$, $i = 1, 2, \ldots, m$. In each partition i one obtains three local functions y_i, z_i, and Δ_i. The first two are identical to the ones obtained for the homogeneous case (driven by the function $\sin(kr)$ and $\cos(kr)$). They obey the equations

$$\mathcal{O}_i y_i = \sin(kr), \qquad \mathcal{O}_i z_i = \cos(kr),$$

where $\mathcal{O}_i$ is the operator $I - \mathcal{G}_0 V_L$, which symbolically represents the expression given by Eq. (3.1) of Ref. [1]. The third function is the solution of

$$\mathcal{O}_i \Delta_i = \chi_i, \tag{69}$$

where

$$\chi_i(r) = -(\mathcal{G}_0\mathcal{I})_i = \frac{1}{k}\cos(kr)\int_{b_{i-1}}^{r}\sin(kr')\mathcal{I}(r')\,dr' + \frac{1}{k}\sin(kr)\int_{r}^{b_i}\cos(kr')\mathcal{I}(r')\,dr'. \tag{70}$$

By writing out the integral over $\mathcal{G}_0$ in Eq. (68), one finds that

$$\mathcal{O}_i\psi_i(r) = A_i\sin(kr) + B_i\cos(kr) + \chi_i(r), \qquad b_{i-1} \le r \le b_i,$$

from which it follows that

$$\psi_i(r) = A_i y_i(r) + B_i z_i(r) + \Delta_i(r). \tag{71}$$

According to Eq. (68), the coefficients A_i and B_i satisfy the relations

$$A_i = 1 - \frac{1}{k}\int_{b_i}^{T}\cos(kr')(V_L(r')\psi(r') - \mathcal{I}(r'))\,dr'$$

$$B_i = -\frac{1}{k}\int_{0}^{b_{i-1}}\sin(kr')(V_L(r')\psi(r') - \mathcal{I}(r'))\,dr'.$$

Replacing $\psi(r')$ in the above expressions by Eq. (71) and decomposing the integrals into sums over the integrals in each interval, one obtains a matrix equation for the coefficients A_i and B_i. By rearranging rows and columns, in a manner identical to what led to Eq. (3.11) of [1], one finally obtains

$$M\begin{pmatrix}\alpha_1\\ \alpha_2\\ \vdots\\ \vdots\\ \alpha_{m-1}\\ \alpha_m\end{pmatrix} = \begin{pmatrix}0\\ 0\\ \vdots\\ \vdots\\ 0\\ u\end{pmatrix} + \begin{pmatrix}d_1\\ d_2\\ \vdots\\ \vdots\\ \vdots\\ d_m\end{pmatrix}, \tag{72}$$

where the "big" matrix M is identical to the one given for the homogeneous case, and the vectors α_j, u, 0, and d_j are

$$\alpha_j = \begin{pmatrix}A_j\\ B_j\end{pmatrix}; \qquad u = \begin{pmatrix}1\\ 0\end{pmatrix}; \qquad u = \begin{pmatrix}0\\ 0\end{pmatrix}; \tag{73}$$

$$d_j = \begin{pmatrix}-(c\Delta)_{j+1} + \gamma_{j+1}\\ -(s\Delta)_{j-1} + \sigma_{j-1}\end{pmatrix}. \tag{74}$$

Here, by definition,

$$(c\Delta)_p = \frac{1}{k}\int_{b_{p-1}}^{b_p}\cos(kr)V_L(r)\Delta(r)\,dr,$$

$$(s\Delta)_p = \frac{1}{k}\int_{b_{p-1}}^{b_p}\sin(kr)V_L(r)\Delta(r)\,dr$$

$$\gamma_p = \frac{1}{k}\int_{b_{p-1}}^{b_p} \cos(kr)\mathcal{I}(r)\,dr,$$

$$\sigma_p = \frac{1}{k}\int_{b_{p-1}}^{b_p} \sin(kr)\mathcal{I}(r)\,dr.$$

In the above it is assumed that $(s\Delta)_p = \sigma_p = 0$ for $p = 0$, $(c\Delta)_p = \gamma_p = 0$ for $p \geq m$.

Equations (72)–(74) are the main result of this appendix. They show that the coefficients A_i and B_i have three components. One component, $A_i^{(0)}$ and $B_i^{(0)}$, is identical to the solution of the homogeneous equation, and gives rise to the solution of the corresponding homogeneous Schroedinger equation, denoted as F below. The other component, $A_i^{(\mathcal{I})}$ and $B_i^{(\mathcal{I})}$, driven by the column containing the d_j's, gives rise to a special solution of the inhomogeneous equation.

At large distances where the potential and the inhomogeneous term go to zero, the coefficients $A_i^{(0)} \to 1$, $A_i^{(\mathcal{I})} \to 0$ for $i \simeq m$, while the coefficients B_i approach constant values. Hence asymptotically the main effect of the inhomogeneous term is to change the constant in front of $\cos(kr)$, while at small distances the wave function changes due to the non-zero values of $A_i^{(\mathcal{I})}$, $B_i^{(\mathcal{I})}$, and Δ_i.

Formally this result can be understood as follows. The effect of the inhomogeneous term $\mathcal{I}(r)$ is usually obtained by first defining a Green's function which includes the distortion due to V_L, $\mathcal{G}_V = (d^2/dr^2 - V_L + k^2)^{-1}$, and then applying this operator upon $\mathcal{I}$. By making use of the well known relation between $\mathcal{G}_V$ and $\mathcal{G}_0$,

$$\mathcal{G}_V = (1 - \mathcal{G}_0 V_L)^{-1}\mathcal{G}_0 = (1 + \Omega)\mathcal{G}_0, \tag{75}$$

where

$$\Omega = (1 - \mathcal{G}_0 V_L)^{-1}\mathcal{G}_0 V_L,$$

one finds that

$$\psi = F + \chi + \Omega\chi. \tag{76}$$

Here χ was defined in Eq. (68), and F is the solution of the homogeneous equation (Eq. (67) with $\mathcal{I} = 0$), which in the partition i is given by

$$F(r) = \phi + \Omega\phi = \phi(r) + A_i^{(0)} Y_i(r) + B_i^{(0)} Z_i(r), \tag{77}$$

with $\phi = \sin(kr)$. From Eq. (77) above one concludes that $(\Omega\phi)_i$ is equivalent to the numerical procedure which leads to $A_i^{(0)} Y_i + B_i^{(0)} Z_i(r)$. Hence the term $\Omega\chi$ in Eq. (76) is equivalent to that part of $A_i^{(\mathcal{I})} Y_i + B_i^{(\mathcal{I})} Z_i(r)$ which is given by the terms due to γ and σ in Eq. (72), and the term χ in Eq. (76) is due to the combination of Δ and the terms $(c\Delta)$ and $(s\Delta)$ in Eq. (72).

REFERENCES

1. R. A. Gonzales, J. Eisert, I. Koltracht, M. Neumann, and G. Rawitscher, Integral equation method for the continuous spectrum radial Schroedinger equation, *J. Comput. Phys.* **134**, 134 (1997).
2. J. Weiner, V. S. Bagnato, S. Zilio, and P. S. Julienne, Experiments and theory in cold and ultracold collisions, *Rev. Mod. Phys.* **71**, 1 (1999).

3. M. F. Rasamny, M. Valiev, and G. Fernando, *Phys. Rev. B* **58**, 9700 (1998); Y. Hahn, *Phys. Rev. A* **55**, 4238 (1997).
4. L. D. Faddeev, The inverse problem in the quantum theory of scattering, *Russian Math. Surveys* **14**(4), 57 (1959).
5. R. H. Landau, *Quantum Mechanics. II. A Second Course in Quantum Theory* (Wiley–Interscience, New York, 1989).
6. L. I. Schiff, *Quantum Mechanics*, 3rd ed. (McGraw–Hill, New York, 1968).
7. R. W. Hamming, *Numerical Methods for Scientists and Engineers* (McGraw–Hill, New York 1962).
8. C. W. Clenshaw and A. R. Curtis, A method for numerical integration on an automatic computer, *Numer. Math.* **2**, 197 (1960).
9. L. Greengard and V. Rokhlin, On numerical solution of two-point boundary value problems, *Comm. Pure Appl.* **44**, 419 (1991).
10. D. Gottlieb and S. Orszag, *Numerical Analysis of Spectral Methods* (SIAM, Philadelphia, 1977).
11. G. H. Golub and C. H. Van Loan, *Matrix Computations* (Johns Hopkins Press, Baltimore, 1983).
12. M. Abramovitz and I. Stegun (Eds.), *Handbook of Mathematical Functions* (Dover, New York, 1972).
13. C. Van Loan, *Computational Framework for Fast Fourier Transform* (SIAM, Philadelpia, 1992).
14. L. M. Delves and J. L. Mohamed, *Computational Methods for Integral Equations* (Cambridge Univ. Press, Cambridge, UK, 1985).
15. J. Stoer and R. Bulirsch, *Introduction to Numerical Analysis*, 2nd ed. (Springer-Verlag, New York, 1993).
16. T. E. Simos, *J. Comput. Math.* **14**, 120 (1996).
17. T. E. Simos and P. S. Williams, *Comput. Chem.* **21**, 175 (1997).
18. G. H. Rawitscher, B. D. Esry, E. Tiesinga, P. Burke, Jr., and I. Koltracht, Comparison of numerical methods for the calculation of cold atoms collisions, *J. Chem. Phys.*, submitted.
19. M. Marinescu, H. R. Sadeghpour, and A. Delgarno, *Phys. Rev. A* **49**, 892 (1994).